

FINITE ELEMENT ANALYSIS OF THE SCAPHOID IN A FALLING ONTO OUTSTRECHED HAND SCENARIO

MASTERS THESIS 9700

LIEM LUONG

ACADMEIC SUPERVISOR: DR RAMI AL-DIRINI

Submitted to the College of Science and Engineering in partial fulfilment of the requirements for the degree of Bachelor of Engineering (Biomedical) (Honours), Master of Engineering (Biomedical) at Flinders University – Adelaide Australia

I certify that this thesis does not incorporate without acknowledgement any material previously submitted for a degree or diploma in any university; and to the best of my knowledge and belief it does not contain any material previously published or written by another person except where due reference is made in the text.

Signed: 

Date: 24/12/2021

Table of Contents

Abstract	3
Acknowledgements	4
Introduction	5
Literature Review	6
Gap	8
Methodology	10
FE Numerical Results	18
Unsmoothed	18
Ligaments.....	18
No Ligaments	18
Ligaments vs No ligaments.....	18
Smoothed	19
Ligaments.....	19
No Ligaments	19
Smoothed ligaments vs Smoothed no ligaments	20
Smoothing vs Unsmoothed.....	20
Ligaments.....	20
No Ligaments	20
FE Analysis Results – Stress Distribution	22
Ulnar View	22
Radial View	25
FE Analysis Results – Strain Distribution	28
Ulnar View	28
Radial View	31
Discussion	35
Conclusion	40
Future work	40
References	42
Appendix: Core MATLAB Program	46
Appendix: Function to Map Ligaments to a Delaunay Triangle Mesh	50

Table of Figures and Tables

Figure 1: Comparison of the same wrist when scanned by x-ray and MRI. On the x-ray, there is no visible fracture, however, for a T2 and T1 weighted MRI, the scans show a clear fracture line which was obscured by in the x-ray	5
Figure 2: Left: mapping of common fracture patterns on a scaphoid model. Right: mapping of uncommon fracture patterns on a scaphoid model.	5
Figure 3: MATLAB screenshot of the variable table showing the CT scan data of each scaphoid	11
Figure 4: Nodal positions of the first 12 nodes. The columns represent the x, y, z coordinates going left to right.....	11
Figure 5: List of HU units of the first 12 nodes	12
Figure 6: MATLAB screenshot of the output of the ConstrainedDelaunayTriangle	12
Figure 7: MATLAB screenshot of the resultant mesh, which is a direct output from the Delaunay triangulation	12
Figure 8: MATLAB screenshot of the first 12 element definitions. The rows contain corresponding node numbers of the elements.....	13
Figure 9: MATLAB screenshot of the table containing Young's Modulus values of the first 12 elements in terms of individual nodal Young's Modulus of Elasticity	Error! Bookmark not defined.
Figure 10: MATLAB screenshot describing the Young's Modulus of Elasticity which are averaged from the Young's Modulus of the constituent nodes	Error! Bookmark not defined.
Figure 11: Example of mapping from the statistical model to a scaphoid shape. The blue dots represent the mapped nodes from the statistical model and the mesh is a scaphoid model. The image shows an uneven distribution of node mapping	15
Figure 12: The four graphs show the change in maximum strain when increasing the mesh volume in all simulation types. There appears to be negative correlation.	34
Figure 13: The four graphs show the change in maximum stress when increasing the mesh volume in all simulation types. There appears to be negative correlation.	34
Figure 14: When using the current method of mesh smoothing, artifacts are created on the mesh surface which include irregular change to scaphoid shape (blue arrow and poor element shape)	36
Table 1: Table describing the format in which the material properties, nodal positions, element definitions, element sets and node sets are defined in a .inp file to be loaded into a FEA program ..	16
Table 2: Table describing the format which the forces acting for each node set are defined in a .inp file.....	16
Table 3: Table describing the distribution of stress and strain in simulations have unsmoothed meshes and ligament simulations.....	18
Table 4: Table describing the distribution of stress and strain in simulations have unsmoothed meshes and no ligament simulations.....	18
Table 5: Table describing the change in stress and strain distribution after simulating ligaments in unsmoothed meshes	18
Table 6: Table describing the distribution of stress and strain in simulations have smoothed meshes and ligament simulations.....	19
Table 7: Table describing the distribution of stress and strain in simulations have smoothed meshes and no ligament simulations.....	19
Table 8: Table describing the change in stress and strain distribution after simulating ligaments in smoothed meshes.....	20
Table 9: Percentage change in stress and strain distributions when smoothing the mesh in simulations with ligaments	20

Table 10: Percentage change in stress and strain distributions when smoothing the mesh in simulations without ligaments.....	21
Table 11: Table containing FEBio screenshots of the stress heatmaps in the ulnar view of all simulations.....	22
Table 12: Table containing FEBio screenshots of the stress heatmaps in the radial view of all simulations.....	25
Table 13: Table containing FEBio screenshots of the strain heatmaps in the ulnar view of all simulations.....	28
Table 14: Table containing FEBio screenshots of the strain heatmaps in the radial view of all simulations.....	31

Abstract

Plain radiographs are the first imaging technique used to determine the presence of a scaphoid fracture. Due to the alignment of the fracture orientation and radiograph plane, scaphoid fractures can be missed. There are no current methods to determine the orientation of scaphoid fractures prior to an x-ray. Previous analysis of the wrist and scaphoid have not measured the stress and strain distributions on the scaphoid and investigated the influence of simulating wrist ligaments on finite element solutions. To investigate the stress and strain distributions on the scaphoid, 8 finite element models of the scaphoid from CT data from Brown University created in MATLAB were analysed in a falling onto outstretched hand with radial deviation scenario using FEBio. To investigate the influence of ligaments on FE analysis of the scaphoid, ligament attachment sites are mapped onto the scaphoid using a statistical model, iterative closest point algorithms and knnsearches and small tensile forces are applied at the mapped locations. In all simulations, the most significant stresses and strain occurred on the dorsal edge of the scaphoid. When comparing simulations between models with and without ligaments, the addition of ligaments was found to decrease the minimum stress and strains in unsmoothed models by 13.04% and 11.02%, and 11.4% and 14.8% in smoothed models. When comparing the influence of smoothing the mesh, there is a significant decrease in stress and strain distributions in both ligament and no ligament simulations. Due to the lack of scaphoid specific patient information, the same force was applied to all scaphoids, therefore the numerical stress and strain distributions are difficult to analyse, however, the stress and strain patterns are similar to common fracture patterns where the most significant stress and strains are on the dorsal side of the scaphoid. Although there is a significant numerical increase in minimum stress and strain due to ligament simulation, there is no or little statistical significance in the changes therefore, the effect of ligament simulation was found to be insignificant overall. In the smoothing process of the meshes, there is an increase in volume of each model, which is likely to be the cause of observed decrease in stress and strain, however, further analysis is required. Future work on simulations of stress and strain simulations on the scaphoid will require the better assumptions and application of the ligament and falling force vectors.

Acknowledgements

A special thanks to Flinders University and Dr. Rami Al-Dirini for providing the opportunity to take on the project. Prof. Greg Bain and Melanie with assistance with ligament mapping and project discussions. Marouska for previous work with Rami Al-Dirini regarding PCA of the scaphoid.

Brown University provided segmented CT scan data of scaphoids.

Introduction

The scaphoid plays a major role in the biomechanics of the wrist, thus, is the most fractured carpal bone following a fall onto outstretched hands (K. Garala, et al., 2019, R. Sendher, et al. 2013). Initial scaphoid fracture predictions are based on clinical presentations include local tenderness around the scaphoid area and compression of the thumb (R. Sendher, et al., 2013). Patients with a suspected scaphoid fracture have their wrist immobilised before an x-ray is performed on the wrist (S. Rhemrev, 2011). The treatment plan is reviewed based on visible presence of a fracture in the x-ray image and on patient symptoms. However, based on the scaphoid fracture orientation, the fracture can be obscured and difficult to be visually detected due to the imaging mode. This can be demonstrated in Figure 1.

Figure removed due to copyright restriction

Figure removed due to copyright restriction

Figure 1: Comparison of the same wrist when scanned by x-ray and MRI. On the x-ray, there is no visible fracture, however, for a T2 and T1 weighted MRI, the scans show a clear fracture line which was obscured by in the x-ray

Due to the misalignment, scaphoid fractures can be missed and can lead to misinterpretation where patients are given a false positive scaphoid fracture prediction. For patients given false positives, they will experience long periods of wrist immobilisation, which will significantly affect their lives. In contrast, for patients with negative x-rays, but have a scaphoid fracture, they must wait for another period of time before a second radiograph is taken to look for the presence of comminution (S. Rhemrev, 2011). With comminution, the treatment plan can either involve surgery due to the long period between when the fracture was sustained and the accurate diagnosis of a fracture.

Some of the most common fracture patterns are shown in Figure 2. These are common and uncommon fracture patterns mapped onto a scaphoid model (A. Turrow, et al. 2019). From these figures, scaphoid fracturing can occur at different locations and orientations.

Figure removed due to copyright restriction

Figure removed due to copyright restriction

Figure 2: Left: mapping of common fracture patterns on a scaphoid model. Right: mapping of uncommon fracture patterns on a scaphoid model.

To improve patient outcomes in scaphoid treatment, making a more accurate initial prediction is important. This project aims to investigate the use of finite element analysis to observe stress and strain distribution in scaphoids following a fall onto outstretched hand scenario.

Literature Review

Scaphoid fracture predictions are based on presence of clinical symptoms and patient descriptions on falling technique (M. Mack, 2002, W. Mallee, S. Rhemrev, 2011). However, predicting scaphoid fractures only on those two criteria does not correctly identify scaphoid fracturing in every case, thus a follow up X-ray is taken to visually confirm the presence of a fracture (M. Mack, 2002). Between the clinical visit and first x-ray, the wrist of suspected scaphoid fracture patients is immobilised, significantly impacting their ability to perform daily tasks (S. Rhemrev, 2011), despite a scaphoid fracture not being confirmed. The x-ray is taken in two planes to image the scaphoid fracture, however, in many cases, the fracture can be missed due to the alignment of the scaphoid fracture with plane of the fracture (M. Mack, 2002), leading to incidents of false negatives. Due to difficulty in determining scaphoid fractures based on X-ray imaging, patient is predicted to have a scaphoid fracture based on clinical presentation and falling mechanism (W. Mallee, 2019). In cases where the first x-ray shows a negative radiograph, a secondary radiograph image is taken.

One method of reducing the number of false negatives at the clinical presentation stage is to use a detection rule which weights clinical presentations and patient information to predict likelihood of a fracture (M. Mack, 2002). Although the formula was found to improve fracture predictions, false positives were still made. A method of reducing immobilisation period and predicting fracture earlier in the treatment process, is to perform an MRI scan (C. Bakker, 2017). MRI is found to significantly improve scaphoid fracture compared to X-ray scans, increasing confidence of presence of scaphoid fractures (M. Mack, 2002). Despite the clinical improvements to scaphoid fracture predictions, using an MRI scan as the first radiograph technique is unrealistic. Computed tomography (CT) is another technique to determine scaphoid fracturing. As CT scans are three dimensional, the ability to reformat the CT scan to a different plane can aid in determining scaphoid fractures (A. Cheema, 2018). However, CT scans will expose patients to more radiation compared to an x-ray (Akram and Chowdhury, 2020), making CT scans less desirable as an imaging modality.

Finite element analysis (FEA) of bone can be performed to predict bone biomechanics based on different loading conditions. With the correct assumptions (boundary and loading conditions) bone biomechanics be predicted. FEA of bone can be used to directly predict stress and strain predictions (Y. Lee, 2019), fracture propagation (R. Hambii, 2011) or be used as preliminary research for future analytical processes (S. Martelli, 2018).

FEA of the wrist has been performed on FE models of the wrist (A. Iananmardian, 2010, Y. Matsuura, 2017) and scaphoid (P. Varga, 2015, 2017) based on CT and microCT scans. In FE models of the wrist the full wrist is scanned and loads at the distal carpal bones whereas in scaphoid models, the loads are applied at specific locations on the scaphoid. The variance between techniques results in varying levels of complexity for each method. In models involving the whole wrist, the contact surfaces are predicted in FE, whereas in a scaphoid model, carpal bone contact must be modelled manually.

In FE analysis, the more accurate the model, the more accurate the results. For models such as the femur, modelling the muscular attachments is significant in both the addition of muscular attachments and forces as well as the methodology of applying the loads (K. Polga, 2003). Although the scaphoid does not have any muscular attachments, the scaphoid has many ligament attachments, mapped by Buijze, et al. (2011), Nagao, et al. (2005), Nanno, et al. (2006), Nanno, et al. (2007), and Kijima, et al. (2009). Although the forces of the ligaments may not be significant in physiological movements (scapholunate interosseous ligament (SLIL): 20N in dart throwing motion (Dimitris, et al., 2015) and 44.5N in push up position (L. Scordino, 2016)), the maximum load which the ligaments can bear can become significant (maximum SLIL: 147N (F. Nikolopoulos, 2011),

maximum dorsal radiocarpal ligament (DRC): 143N, maximum dorsal intercarpal ligament (DIC): 82N (S. Viegas, 1999)). Based on the primary protein composition of ligaments (parallel collagen fibres), the ligaments will create tensile forces (J. Kuhlmann, 1990). In a falling scenario, there are cases where the ligament can rupture and fail, thus applying a load equivalent to the maximum load of the ligament. However, the predicted maximum load a ligament can bear is dependent on the testing technique, thus, has significant variation in the results (F. Nikolopoulos, 2011).

Apart from producing forces on the scaphoid, the ligaments can also have significant impacts on the stabilisation of carpal joints, such as the SLIL being the primary stabiliser for scaphoid and lunate movement and the transverse carpal ligament TCL being a significant stabilizer of the carpal arch ((M. Holmes, 2011), (M. Tengrootenhuysen, 2009)).

There is limited research regarding the influence of ligaments FEA to predictions stresses and strains in the scaphoid bone. Iananmardian (2010), investigated the influence of ligaments in a grasping position and found no significant difference compared to previous literature when modelling ligament in the wrist on peak FE inter-carpal joint contact forces. P. Varga, et al. simulated carpal contact area and ligament attachments (forces are between 0.24N and 16.04N) in a wrist model, however, did not compare results to simulations with no ligaments.

The force due to falling onto an outstretched hand will be the most significant force being applied onto the scaphoid. There is little literature regarding the force the scaphoid is exposed to in a falling force. Lee suggests using a factor of body weight to apply to the scaphoid and whereas R. Kiss uses a strain rate of 700mm / min. When applying a load to the wrist, the distribution of force between the scaphoid and lunate must be considered. In experimental testing, M. Majima, et al., 2007, found 62% of the force of the palm is transmitted through the scaphoid in an extended position. In FE simulations, Iananmardian, 2010 found 55% of the force produced in a grasping scenario is transmitted through the scaphoid.

Within FEA, the material properties (Young's Modulus of elasticity, density and poisson's ratio) must be defined. For data from CT scans, the Hounsfield units (HU) per voxel can be converted to density, then to Young's Modulus through equations relating HU to density, and density to Young's Modulus (E. Morgan, 2003). However, based on anatomical site and range of HU, the material property definitions will not always be accurate (I. Fleps, 2020), therefore the predicted material properties must be validated or calibrated. Another consideration which must be made is comparing the results to numerical results. It is possible that, although the predicted FE results are accurate for one criterion, the FE results can be poor against other criteria (L. Cyganik, 2014). Determining material property relationships can be performed using manual calculations of the material property equations and validation with numerical results, however, the use of external programs such as ScanIP can give reliable results (R. Gujar, 2020).

Bone is known to be anisotropic, with different areas having greater degrees of anisotropy depending on anatomic site (e.g. trabecular bone compared to cortical bone) (S. Kazembakhshi, 2014). Within the femoral head, the use of microCT can be used predict anisotropic direction with the bone (W. Enns-Bray, 2014). Being able to model the anisotropic material properties would make the model more accurate, however would significantly increase the complexity of the model, therefore would require more resources to solve each simulation (W. Enns-Bray, 2014). Overall, FE models were found to be less sensitive to anisotropic material properties (W. Enns-Bray, 2014), (A. Synek, 2015), therefore may not be a worthwhile use of resources.

Another significant property of bone is the inhomogeneous material properties. At different locations, there can be differing variations in material content (e.g. fat, hydroxyapatite, etc.) (L. Cyganik, 2017, A. Sudhyadhoml, 2020), therefore bone will have different material properties from one location to another. Material property definitions can be adjusted to obtain better material property predictions (A. Sudhyadhoml, 2020, J. Macneil, 2007, L. Cyganik, 2017), however, will require the ability to reliably determine material composition of the bone. In addition, due to fat content in the bone, the HU value of each voxel in a CT scan can be lower than expected (J. Vivanco, 2014), therefore, material property equations must be used carefully.

In an FE model, inhomogeneous material properties can be modelled by converting individual voxels from a CT scan to local material properties (S. Martelli, 2018) and homogenous material properties can be modelled by associating all elements of a certain position to have the same material properties (A. Synek, 2015). When comparing FE results to numerical results, (A. Synek, 2015), found modelling inhomogeneous material properties to create more accurate results compared to modelling homogenous material properties.

The inhomogeneous material properties can be associated with the difference between cortical and trabecular bone. Both bone types have significantly different levels of bone material densities and material compositions. As a result, both bone types must be modelled differently to produce accurate bone modelling. To achieve this, cortical bone and trabecular bone can be given different material property equations (S. Kazembakhshi, 2014). Using a single equation based on literature is unlikely to be reliable due to the range of HU or densities that the equation applies to (I. Fleps, 2020). The significance for modelling cortical and trabecular bone differently is due to cortical and trabecular bone bearing loads differently (J. Macneil, 2007), (C. Turner, 1998), therefore using incorrect bone equations result in changes in load bearing capabilities of the bone types.

Another key definition for FE analysis is the boundary condition, which will define nodes that will be defined to have no movement. For the scaphoid, this will be the radioscapoid joint. In falling scenario, the wrist will go into an extended position and the falling force will be applied to the distal scaphoid (Y. Chen, 2013). When in the extended position, the radioscapoid joint will act on the dorsal, proximal articular surface (Y. Chen, 2013, J. Tang, 2012) of the scaphoid.

Regarding literature on scaphoid fractures, previous literature have described fracture locations on a general scaphoid (K. Garala, et al. 2019, A. Turrow, et al. 2020, A. Bulstra, 2021) in terms of orientation of fracture on the scaphoid. There has been a preliminary study which modelled the wrist in a falling scenario using a strain rate of 700 mm / min on a single wrist model (R. Kiss, 2020). Another study FE modelled the wrist for Smith's fractures and produced a model which could look at scaphoid fracture patterns, however, scaphoid stress and strain analysis was part of the preliminary research, thus no conclusions were made for scaphoid fracturing. There are few to no papers which have looked at stress and strain distributions on the scaphoid in FE or experimental.

Gap

Fracture predictions of the scaphoid have not been directly analysed using FE models. Previous studies have either looked at fracture patterns of the scaphoid in one specific case with the whole wrist model or looked at scaphoid fracture orientation on a standard scaphoid model. There are no studies which have used finite element analysis to predict stress and strain distributions on the scaphoid. Some studies have looked at peak stresses and strains, but none have looked at the distributions as a primary goal. There are even less studies which have looked at the reaction of the

scaphoid and wrist in a falling scenario, therefore the stress and strain distributions on the scaphoid have not been analysed in a falling scenario.

The modelling and contribution of ligaments on the scaphoid have not been analysed in literature. In FE simulations of the wrist, some studies have not modelled ligaments on the scaphoid whereas some others have. Very few studies have been performed on evaluating the influence of modelling accurate wrist biomechanics. As a result, there is gap in the prediction of the influence of ligaments in an FE model of the scaphoid.

Determining accurate ligament influence on the scaphoid have not been analysed in literature. There is significant literature on the functionality of various ligaments on the scaphoid, however, there are studies which have analysed the ligament reactions in the wrist in a falling scenario. As such, there is a gap in the understanding of the ligament influence in a falling scenario. Bulstra, et al, have predicted the influence of ligaments in a scaphoid fracturing scenario, however, further research is necessary to verify these predictions.

Methodology

Overview

Below is an overview of the steps taken to accomplish the project.

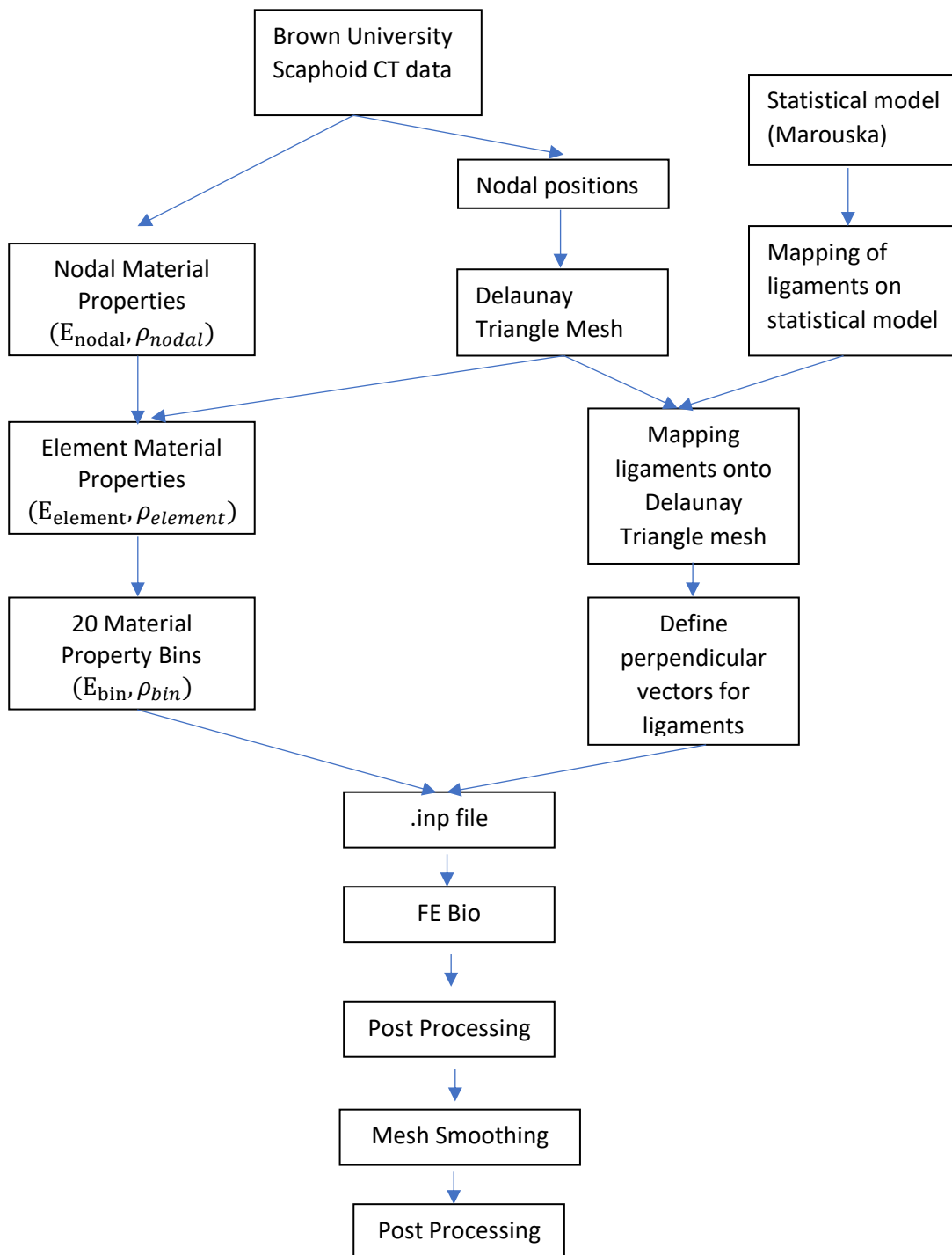


Figure 3: Flow diagram of the project (steps taken in the project)

Data analysis

Brown University provided MATLAB data of CT scans of the wrist. The MATLAB data contains data as per the figure below:

Name	Size	Bytes	Class
NIn	42x81x28	190512	int16
Nsmall	42x81x28	190512	int16
ref_Small	1x1	328	imref3d
wrLs	1x1	1032246	struct

Figure 4: MATLAB screenshot of the variable table showing the CT scan data of each scaphoid

The three most important variables within this data and their associated relevance for the project are:

- NIn: Hounsfield values of the CT scan of the scaphoid. This data is most likely segmented data from Nsmall
- Nsmall: Hounsfield values of the CT scan of the wrist
- Ref_Small: Contains variables which relate the intrinsic coordinates of the 3D matrices to the original CT pixel size (e.g. pixel size, image size, etc.)

For the simplicity of the project, NIn will be used such that automatic segmentation would not be necessary to try to isolate the scaphoid from the rest of the scan data in Nsmall. There was an attempt to use clustering with Nsmall, however, due to the tweaking necessary to get the clustering to work, it would be more efficient to just use NIn.

Nodal list creation

The first step to creating a mesh is to obtain a node position list for all the points in the matrix containing Hounsfield units which are above a threshold of 100, which was part of the initial segmentation MATLAB code. The threshold was left in as a value of 100 should not have any significant affect of the node like creation. In order to convert the intrinsic coordinates from the matrix to the global coordinates, the (x,y,z) coordinates are multiplied with their respective pixel size (PixelExtentInWorld). The x and y pixel sizes are 0.3906mm and the z pixel size is 0.6350mm. In MATLAB, this is achieved by creating a loop that will check all positions within the matrix and for any position with a value greater than 0, the x, y and z coordinates are multiplied with their respective pixel size and concatenated onto the existing node list. This will produce a list where the row number of the list will correspond to the node number.

	1	2	3
1	0.7813	14.4531	10
2	0.7813	14.4531	10.6250
3	0.7813	14.8438	9.3750
4	0.7813	14.8438	10
5	0.7813	14.8438	10.6250
6	0.7813	15.2344	9.3750
7	0.7813	15.2344	10
8	0.7813	15.2344	10.6250
9	0.7813	15.6250	9.3750
10	0.7813	15.6250	10
11	0.7813	15.6250	10.6250
12	0.7813	16.0156	9.3750

Figure 5: Nodal positions of the first 12 nodes. The columns represent the x, y, z coordinates going left to right

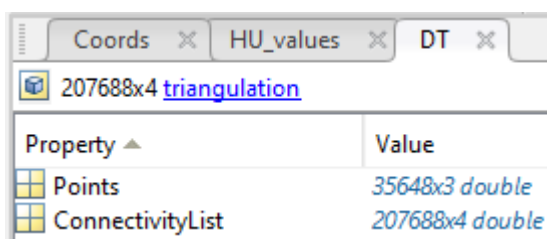
In addition, a list of Hounsfield units is also created using the same loop as the node position list, such that the position in the matrix corresponds to the node it is associated with.

HU values 30678x1 int1

Figure 6: MATLAB screenshot of HU_values variable. The rows indicate the number of nodes and columns represent the HU values of the corresponding nodes.

Mesh Creation

The mesh of the scaphoid is created using the constrained Delaunay Triangle function which is part of the open-source GIBBON library (Moerman, Kevin M). In order to use the ConstrainedDelaunayTriangle, there are two inputs required, the node list and a variable describing the connectivity of the surface of the mesh. To create the surface connectivity, the boundary function is used, which requires the node list and a 'shrink factor'. This shrink factor is used to describe how closely the 'boundary' will be to the point cloud and will be set to 0.99. The ConstrainedDelaunayTriangle will produce a triangulation variable which contains the element definitions (ConnectivityList) and the associated node list (Points).



Property	Value
Points	35648x3 double
ConnectivityList	207688x4 double

Figure 7: MATLAB screenshot of the output of the ConstrainedDelaunayTriangle

To ensure the meshing works as expected, the mesh was plotted in MATLAB using the trimesh function (Figure 8).

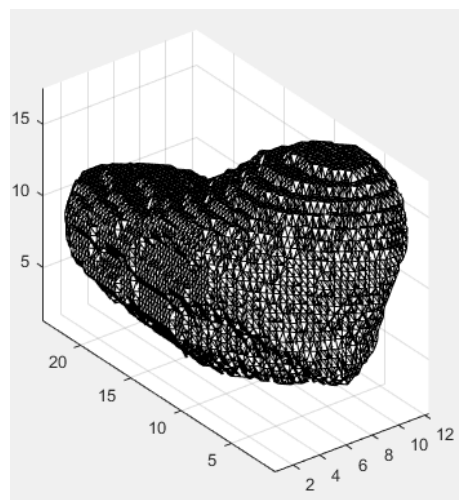


Figure 8: MATLAB screenshot of the resultant mesh, which is a direct output from the Delaunay triangulation

Element property definitions

Defining the material properties for the mesh will come in three stages

1. Creating nodal material definitions
2. Creating element material definitions
3. Creating material property bins

Nodal material properties are created using the following formulas (E. Morgan, et al. 2003):

$$\rho_{nodal} = \frac{1.6990}{\max(HU) - \min(HU)} \times HU_{nodal} \frac{g}{cm^3} \quad (1)$$

$$E = 14664\rho_{nodal}^{1.49} MPa \quad (2)$$

Element material properties are determined by finding the average material properties of the constituent nodes based on the ConnectivityList created as the output of the ConstrainedDelaunayTriangle function. To achieve this in MATLAB, two matrices are made based on the ConnectivityList which contain the Young's Modulus and density of the node at each position of the list (Figure 10). From here, the values in each row are averaged. This produces a list of average material properties for each element (Figure 10).

	1	2	3	4
1	6663	7641	7654	7655
2	10225	10242	11340	10224
3	12380	11220	12381	12401
4	3384	2714	3393	2713
5	20760	20759	20740	19519
6	7554	7570	7555	8543
7	3769	4552	4553	4539
8	898	889	1489	1490
9	632	215	641	208
10	57	295	303	304
11	29651	29971	29985	29972
12	6032	6031	7042	7021

Figure 9: MATLAB screenshot of the first 12 element definitions. The rows contain corresponding node numbers of the elements.

E	30678x1 double
E_bin	1x20 double
E_elem	1x167881 double
E_nodal	167881x4 double

Figure 10: MATLAB screenshot of the variables E, E_bin, E_elem, E_nodal. For E, the rows number corresponds to the node number and the columns E at the corresponding node. For E_nodal, the rows indicate the element number and columns represent E for the nodes of the constituent nodes. For E_elem, the rows indicate the average E for the each node, represented by the column number. The rows of E_bin represent the average E for each material bin where the columns represent bin number.

When exporting all these material properties into ANSYS (ANSYS Workbench, Release R2) or FEBio, both programs would crash without an error message. The solution which was tested to fix this error was to reduce the number of material property definitions by creating material property bins. The chosen value was 20 as an initial limit and was not changed.

The process for creating the material property bins was:

1. Determine material property range per bin
2. Determine what bin each element will belong to
3. Find average material property per bin

As 20 material properties were chosen for the project, the range for each material property bin will be defined as follows:

$$\text{Material property range} = \frac{\max(E_{elem}) - \min(E_{elem})}{20} \quad (3)$$

To determine which bin each element will belong to, the difference between the element Young's Modulus and the minimum Young's Modulus is divided by the material property bin, giving a value between 0 and 20. If the value is rounded off, the range for the bins will be 0:20, thus, the ceiling value is used. The formula will thus be:

$$Element\ Set\ ID = \text{ceil} \left(\frac{E_{elem} - \min(E_{elem})}{Material\ property\ range} \right) \quad (4)$$

Within MATLAB, a list is created to denote the bin ID for each element. Using the bin ID list, Young's Modulus and density lists, the average material properties for each bin ID is determined using:

$$Bin\ Average = \text{mean}(Material\ properties\ of\ Elements\ of\ ID == i) \quad (5)$$

Where 'i' is the loop variable going between 1:20.

This created 2 lists containing 20 values each, where the position in the list corresponds to the average material property of the Bin ID i.e. position 1 is the material property of bin 1.

Ligament mapping must be performed on all models as preliminary step to simulating ligament attachments. The most efficient method to perform the mapping is by mapping the ligaments onto a statistical model which will be morphed onto each individual model.

Defining node sets on statistical model

The areas where the boundary and loading forces will act must be defined based on literature. The boundary condition will act at the proximal scaphoid at an area determined to be the radioscapoid contact area, defined by Tang and Chen (2011). The positions determined to be ligament loading sites are defined by G. Buijze, Dvisnskikh (2011) and Kijima, Veigas (2009). To map these locations, three steps are used:

1. Draw the approximate area on the statistical model
2. Locate the approximate centre/s
3. Use rangeserach to find nodes within a desired distance of each centre

After drawing the approximate area onto an image of the statistical model, the centre is approximated by clicking onto the specific node in a MATLAB trimesh of the scaphoid. As various ligaments are not circular and are more elliptical, multiple centres are defined, where each centre is about half of the approximate width of each ligament away from each other. The area of which the ligament will cover the scaphoid surface is based on literature from G. Buijze (2011), Dvisnskikh, 2011 and visual approximation. The rangesearch function was used to find nodes within a certain radius of a node or node sets. This radius is initially determined by assuming each area is circular and calculating the radius. For mappings with multiple centers, the radius is divided by the number of centers and multiplied by 1.5, to ensure the centers overlap to produce an elliptical mapping shape. These are plotted on the statistical model of the scaphoid and adjustments are made to ensure the mapping appears consistent with literature as some scaphoids can be larger or smaller than each other, thus ligament mapping will not always cover the same surface area. Assistance of drawing the approximate mapping and validation of the mapping process was performed by Prof. Greg Bain.

Ligament mapping from SSM to shape

The ligament mapping is mapped from the statistical model each scaphoid shape using rigid ICP, non-rigid ICP and knnsearches. Rigid ICP is used to align two-point clouds in a way that minimises the distance between each point, thereby aligning the statistical model with the scaphoid shape,

without altering the shape of either nodes. The non-rigid ICP is used to align nodes as closely as possible by deforming one mesh to fit to the other. In both cases, the statistical model is adjusted to fit to the scaphoid shape. As the surface meshes do not have the same number of nodes and the

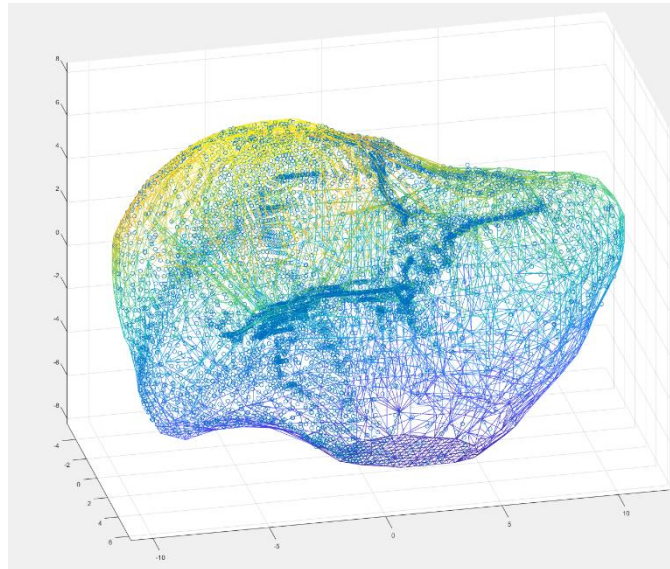


Figure 11: Example of mapping from the statistical model to a scaphoid shape. The blue dots represent the mapped nodes from the statistical model and the mesh is a scaphoid model. The image shows an uneven distribution of node mapping

non-rigid ICP mapping results in nodes being assigned positions not exactly on the nodes of the scaphoid shape, a knnsearch is performed to associate the mapped nodes to a node on the scaphoid shape. This can lead to multiple mapped nodes being associated to a single node, thus only unique nodes will be used.

The mapping is performed in 2 steps:

1. Statistical model to surface nodes defined by boundary function
2. Surface nodes from boundary function to complete node set

The first mapping technique will incorporate the method mentioned above, whilst the second will only require the knnsearch technique as most nodes are already in the correct position or close to.

The mapping portion of the code is all performed in a function, thus, the inputs and outputs must be defined. As it is desirable to save certain figures and plots, the file path is needed alongside the Delaunay Triangle mesh definitions. In terms of the outputs, the node sets indexes for each mapped ligament and boundary condition are saved in a cell variable alongside another cell used to contain the names of each mapped location.

Define vectors

When applying the forces acting on the scaphoid the forces must be acting normally to the scaphoid surface (based on assumptions), thus the force x, y and z components must be determined. In order to determine the direction of each force the unit vector components, the fitNormal function (Dan Couture (2021)) is used. This code will fit a plane to a set of nodes and output the unit vector components to the fitted plane. The fitNormal function is used in conjunction with the outputs of the mapping function to create a variable containing all the unit vector components for all mapped locations. To convert the unit vector components to the desired force per node (create a distributed force), the unit vector components are multiplied with the desired force (i.e. 560 for distal scaphoid and 20 for ligaments) and divided by the number of nodes.

Output model

The scaphoid mesh is exported from MATLAB in the form of an .inp file which defines the nodes positions, element definitions, material properties, element sets (based on material properties) and node sets (based on mapping). From the formulas earlier, the nodal positions are in mm, Young's Modulus in MPa and density is g/cm³. These must be converted to standard metrics. The formatting for each model data is shown in the table below:

Table 1: Table describing the format in which the material properties, nodal positions, element definitions, element sets and node sets are defined in a .inp file to be loaded into a FEA program

Model Information	Format
Material Property Definitions	*SOLID SECTION, ELSET=ELEMENT_ID_, MATERIAL=ELEMENT_ID *MATERIAL, NAME=ELEMENT_ID *ELASTIC, TYPE=ISOTROPIC E, 0.3 *DENSITY rho
Node Coordinates	*NODE Node number, x-coordinate, y-coordinate, z-coordinate
Element Definitions	*ELEMENT, TYPE=C3D4, ELSET=ELEMENT_ID Element number, Node 1, Node 2, Node 3, Node 4
Element sets	*ELSET, ELSET=ELSET NAME ELEMENT SET NAMES
Node Sets	*NSET, NSET= NSET NAME List of nodes

Output ligament and loading forces

A separate file is created to describe the vector components for each force acting on the scaphoid. The format for each of these forces is:

Table 2: Table describing the format which the forces acting for each node set are defined in a .inp file

Node Set forces	*NSET, NSET = NSET NAME X component Y component Z component
-----------------	--

FE Analysis

Finite element analysis was performed using FEBio (Version 1.5, Atheshian GA, Weiss, JA, United States of America). The steps to perform an FE analysis are:

1. Import mesh
2. Define loading conditions
 - a. Based on vector components exported from MATLAB
 - i. Select nodes within a node set
 - ii. Create x, y and z forces for each node set
 - iii. For no ligament analysis: do not define ligament forces
 - iv. For ligament analysis: define ligament forces
 - b. Ensure direction of force is correct for the loading condition
 - i. Falling force is compressive
 - ii. Ligament forces are tensile
3. Define boundary conditions

- a. Select nodes of proximal radioscaphoid joint
 - b. Create a fixed displacement of (0,0,0) for the selected nodes
4. Define type of analysis
 - a. Select static structural
5. Define outputs in log file
 - a. Creates a file which will contain the stresses and strains at each step of the analysis
 - b. Use element solutions
 - c. Principal stresses: s1,s2,s3
 - d. Principal strains: E1,E2,E3
6. Perform FEA
7. Save radial and ulnar view of the solutions at the final step (i.e. 10 (default))

FE Post processing

From initial analysis of the stress and strain distributions, there are areas with significant stresses and strains which are most likely to be boundary stresses and strains, which are not representative of real-world reactions to loading. As a result, the distribution of stresses and strains throughout the scaphoid will be analysed using principal stresses and strains, which were outputted in the previous step. The values are within a document of type 'file' and contain the results at all steps. The results of the last step must be extracted into an excel file and separated into individual columns. Separating the values into columns can be done using the 'Text to columns' function in excel.

The raw results will be copied into excel with the following format (space delimited format):

Element number Principal Stress/Strain 1 Principal Stress/Strain 2 Principal Stress/Strain 3

e.g. 1 1084622 829292.1 -5114427

By selecting the delimiter to be a space, the data is divided into separate columns.

To analyse the stress and strain distributions, the 5th, mean and 95th percentiles were used on the absolute value of stress and strain in MATLAB to filter out the boundary conditions and observe maximum and minimum forces throughout the scaphoid. Within MATLAB, the excel spreadsheets were imported without the element numbers. From here, the prctile and mean functions were used on all columns and rows. The results for all scaphoid simulations with and without ligament considerations were tabulated with the following headings:

- Scaphoid ID
- Maximum (95th percentile) Stress
- Minimum (5th percentile) Stress
- Mean Stress
- Maximum (95th percentile) Strain
- Minimum Strain (5th percentile)
- Mean Strain

Mesh Smoothing

The mesh of scaphoid 14548 has significant sharp vertices around various areas on the surface. This is due to using a shrink factor of 0.99. To smooth out the scaphoid model, a shrink factor of 0.7 was used. Simulations of the scaphoid are performed again using the same methodology as above.

FE Numerical Results

Unsmoothed

Ligaments

Table 3: Table describing the distribution of stress and strain in simulations have unsmoothed meshes and ligament simulations

Scaphoid ID	Max stress (MPa)	Min Stress (MPa)	Mean stress (MPa)	Max Strain ($\mu\epsilon$)	Min Strain ($\mu\epsilon$)	Mean strain ($\mu\epsilon$)
14548	23.718	0.1144	5.831	6152.9	30.03	1594.5
14613	15.29	0.07479	3.760	2490.8	13.72	658.7
14726	12.55	0.0940	3.434	2417.7	16.199	662.4
14818	12.49	0.05590	2.947	2719.8	12.257	681.41
14819	20.00	0.1112	5.1872	3872.6	23.95	1094.3
14874	28.67	0.1124	7.0365	5049.8	26.42	1519.5
15006	13.42	0.0569	3.0687	3125.3	14.92	838.63
15282	21.79	0.0966	5.132	4179.4	17.91	1017.9
Average	18.491	0.089524	4.54955	3751.038	19.42575	1008.418
Std. Dev	5.992412	0.024184	1.473664	1334.968	6.533389	376.0615

No Ligaments

Table 4: Table describing the distribution of stress and strain in simulations have unsmoothed meshes and no ligament simulations

Scaphoid ID	Max stress (MPa)	Min Stress (MPa)	Mean stress (MPa)	Max Strain ($\mu\epsilon$)	Min Strain ($\mu\epsilon$)	Mean strain ($\mu\epsilon$)
14548	23.8936	0.1085	5.7921	6187.1	28.496	1581.9
14613	15.754	0.0709	3.862	2584.1	12.918	675.88
14726	14.14	0.102	3.840	2654.8	17.41	733.56
14818	12.21	0.0458	2.786	2639.9	9.6256	659.26
14819	20.198	0.1107	5.227	3872.6	23.95	1094.3
14874	25.743	0.0891	6.121	5049.8	26.4196	1519.5
15006	13.22	0.0433	2.975	3213.0	10.70	827.51
15282	21.26	0.0797	4.88	4109.3	15.34	976.48
Average	18.30233	0.08125	4.435388	3788.825	18.1074	1008.549
Std. Dev	5.151044	0.02648	1.256	1300.576	7.300068	366.3038

Ligaments vs No ligaments

Table 5: Table describing the change in stress and strain distribution after simulating ligaments in unsmoothed meshes

Scaphoid	$\Delta_{\max stress}$ (%)	$\Delta_{\min stress}$ (%)	$\Delta_{\text{mean stress}}$ (%)	$\Delta_{\max strain}$ (%)	$\Delta_{\min strain}$ (%)	$\Delta_{\text{mean strain}}$ (%)
14548	-0.73492	5.437788	0.671604	-0.55276	5.383212	0.796511
14613	-2.94528	5.486601	-2.64112	-3.61054	6.208391	-2.54187
14726	-11.2447	-7.84314	-10.5729	-8.93099	-6.95577	-9.70064
14818	2.293202	22.0524	5.778894	3.02663	27.33752	3.359828
14819	-0.9803	0.451671	-0.76143	0	0	0
14874	11.37008	26.15039	14.95671	0	0.001514	0

15006	1.512859	31.40878	3.14958	-2.72954	39.43925	1.34379
15282	2.492944	21.20452	5.163934	1.705887	16.75359	4.241766
Mean change (%)	0.220486	13.04363	1.968157	-1.38641	11.02096	-0.31258
Std. dev. (%)	6.316318	13.9724	7.39197	3.727273	15.71028	4.3343
p value	0.6896	0.0495	0.4235	0.3321	0.073	0.9915

Looking at the average change in the principal stress and strains after simulating ligaments, there is very little change in the maximum and average stresses and strains ($\Delta_{max\ stress} = 0.22\%$, $\Delta_{mean\ stress} = 1.97\%$, $\Delta_{max\ strain} = -1.39\%$, $\Delta_{mean\ strain} = -0.313\%$), however, there is significant change in the minimum principal stress and strain ($\Delta_{min\ stress} = 13.04\%$, $\Delta_{min\ strain} = 11.02\%$).

Smoothed

Ligaments

Table 6: Table describing the distribution of stress and strain in simulations have smoothed meshes and ligament simulations

Scaphoid ID	Max stress (MPa)	Min Stress (MPa)	Mean stress (MPa)	Max Strain ($\mu\epsilon$)	Min Strain ($\mu\epsilon$)	Mean strain ($\mu\epsilon$)
14548	21.34	0.1013	5.196	5569.5	27.18	1440.6
14613	13.00	0.0654	3.1970	2173.2	12.05	571.3
14726	13.20	0.105	3.639	2525.5	18.90	709.4
14818	12.00	0.052	2.790	2599.3	11.52	641.4
14819	16.78	0.1024	4.458	3403.9	23.27	974.2
14874	21.787	0.0813	5.040	4730.0	19.10	1158.0
15006	12.49	0.0453	2.743	2876.7	11.63	771.9
15282	19.36	0.0678	4.424	3815.1	13.40	903.6
Average	16.24463	0.077563	3.935875	3461.65	17.13125	896.3
Std. Dev	4.115898	0.023558	0.977456	1183.355	5.942069	290.7815

No Ligaments

Table 7: Table describing the distribution of stress and strain in simulations have smoothed meshes and no ligament simulations

Scaphoid	Max stress (MPa)	Min Stress (MPa)	Mean stress (MPa)	Max Strain ($\mu\epsilon$)	Min Strain ($\mu\epsilon$)	Mean strain ($\mu\epsilon$)
14548	24.28	0.1100	5.869	6276.4	29.81	1620.0
14613	13.94	0.0635	3.3751	2325.9	11.50	300.8
14726	12.59	0.0978	3.4728	2415.1	17.60	679.0
14819	11.75	0.0400	2.629	2497.3	8.801	624.9
14819	17.994	0.1045	4.729	3603.7	23.53	1028.8
14874	20.65	0.0670	4.618	4461.6	13.08	1060.1
15006	12.51	0.0352	2.709	2965.5	8.894	769.3
15282	19.36	0.0612	4.36	3800.7	12.38	890.0
Average	16.63425	0.0724	3.970238	3543.275	15.69938	871.6125
Std. Dev	4.603456	0.028677	1.117638	1339.823	7.497196	388.2044

Smoothed ligaments vs Smoothed no ligaments

Comparing simulation results between smoothed ligament with no ligament simulations.

Table 8: Table describing the change in stress and strain distribution after simulating ligaments in smoothed meshes

Scaphoid ID	$\Delta_{\max stress}$ (%)	$\Delta_{\min stress}$ (%)	$\Delta_{\text{mean stress}}$ (%)	$\Delta_{\max strain}$ (%)	$\Delta_{\min strain}$ (%)	$\Delta_{\text{mean strain}}$ (%)
14548	-12.1087	-7.90909	-11.467	-11.2628	-8.82254	-11.0741
14613	-6.74319	2.992126	-5.27688	-6.5652	4.782609	89.92686
14726	4.845115	7.361963	4.785764	4.571239	7.386364	4.477172
14818	2.12766	30	6.124002	4.084411	30.89422	2.640422
14819	-6.74669	-2.00957	-5.7306	-5.5443	-1.10497	-5.30715
14874	5.506053	21.34328	9.138155	6.015779	46.02446	9.234978
15006	-0.15987	28.69318	1.255076	-2.99444	30.76231	0.33797
15282	0	10.78431	1.46789	0.378878	8.239095	1.52809
Mean change	-1.65996	11.40703	0.037047	-1.41456	14.77019	11.47053
Std. dev.	6.255402	14.06067	6.96737	6.182499	18.89115	32.29287
p	0.4187	0.1002	0.7801	0.4606	0.1532	0.6019

Looking at the average change in the principal stress and strains after simulating ligaments in smoothed models, there is very little change in the maximum and average stresses and maximum strain ($\Delta_{\max stress} = -1.66\%$, $\Delta_{\text{mean stress}} = 0.037\%$, $\Delta_{\max strain} = -1.41\%$) however, there is significant change in the minimum principal stress, minimum and mean strains ($\Delta_{\min stress} = 11.41\%$, $\Delta_{\min strain} = 14.8\%$, $\Delta_{\text{mean strain}} = 11.47\%$).

Smoothing vs Unsmoothed

Ligaments

Percentage differences between smoothed and unsmoothed models with ligaments

Table 9: Percentage change in stress and strain distributions when smoothing the mesh in simulations with ligaments

Scaphoid ID	Max stress (%)	Min Stress (%)	Mean stress (%)	Max Strain (%)	Min Strain (%)	Mean strain (%)
14548	-11.1434	-12.9319	-12.2209	-10.4749	-10.4857	-10.683
14613	-17.6154	-14.3578	-17.6103	-14.6144	-13.8589	-15.2984
14726	4.924242	10.47619	5.633416	4.268462	14.29101	6.625317
14818	-4.08333	-7.5	-5.62724	-4.63586	-6.39757	-6.23792
14819	-19.1895	-8.59375	-16.3571	-13.7695	-2.92222	-12.3281
14874	-31.5922	-38.2534	-39.6131	-6.7611	-38.3246	-31.2176
15006	-7.44596	-25.6071	-11.8739	-8.64185	-28.2889	-8.6449
15282	-12.5517	-42.4779	-16.0036	-9.5489	-33.6567	-12.6494
Mean change	-12.3372	-17.4057	-14.2091	-8.02226	-14.9554	-11.3043
Std. dev.	10.93519	17.37395	12.77019	5.968214	17.59955	10.48774
p value	0.026	0.0397	0.0308	0.0062	0.0653	0.031

No Ligaments

Percentage differences between smoothed and unsmoothed models without ligaments

Table 10: Percentage change in stress and strain distributions when smoothing the mesh in simulations without ligaments

Scaphoid ID	Max stress (%)	Min Stress (%)	Mean stress (%)	Max Strain (%)	Min Strain (%)	Mean strain (%)
14548	1.591433	1.363636	1.310274	1.42279	4.407917	2.351852
14613	-13.0129	-11.6535	-14.4262	-11.1011	-12.3304	-124.694
14726	-12.3114	-4.29448	-10.5736	-9.92505	1.079545	-8.03535
14818	-3.91489	-14.5	-5.97185	-5.71017	-9.36939	-5.49848
14819	-12.2485	-5.93301	-10.5308	-7.46178	-1.78496	-6.36664
14874	-24.6634	-32.9851	-32.5466	-13.1836	-101.985	-43.3355
15006	-5.67546	-23.0114	-9.81912	-8.34598	-20.3058	-7.56662
15282	-9.81405	-30.2288	-11.9266	-8.11956	-23.9095	-9.71685
Mean change (%)	-10.0062	-15.1553	-11.8106	-7.80305	-20.5247	-25.3577
Std. dev. (%)	7.788435	12.50944	9.637852	4.38077	34.38933	42.38434
p value	0.0234	0.0141	0.0256	0.0075	0.1824	0.0664

The effects of using a smaller shrink factor with the MATLAB ‘boundary’ function can be observed in the two above tables. There are significant decreases in stress and strain distributions across all percentiles. The variations range from: -8.02% (max strain) and -17.41% (minimum stress) for ligament simulations and -7.80% (max strain) and -25.3% (mean strain) for simulations without ligaments.

For the most significant results for the project, maximum stress and strain, the effects of smoothing in ligament simulations are -12.3% in maximum stress and -8.02% in maximum strain. For simulations with no ligament there is a -10.0% in maximum stress and -7.80% in maximum strain.

In all simulations, there is significant variation within the results, as seen in the standard deviations in each table.

At the bottom of Tables 5, 8, 9 and 10, the result of pairwise t tests comparing the numerical results are shown. For ligament simulation, the differences between the data are insignificant except for minimum stress in unsmoothed simulations. Overall, there is no statistical difference between simulations with and without ligaments.

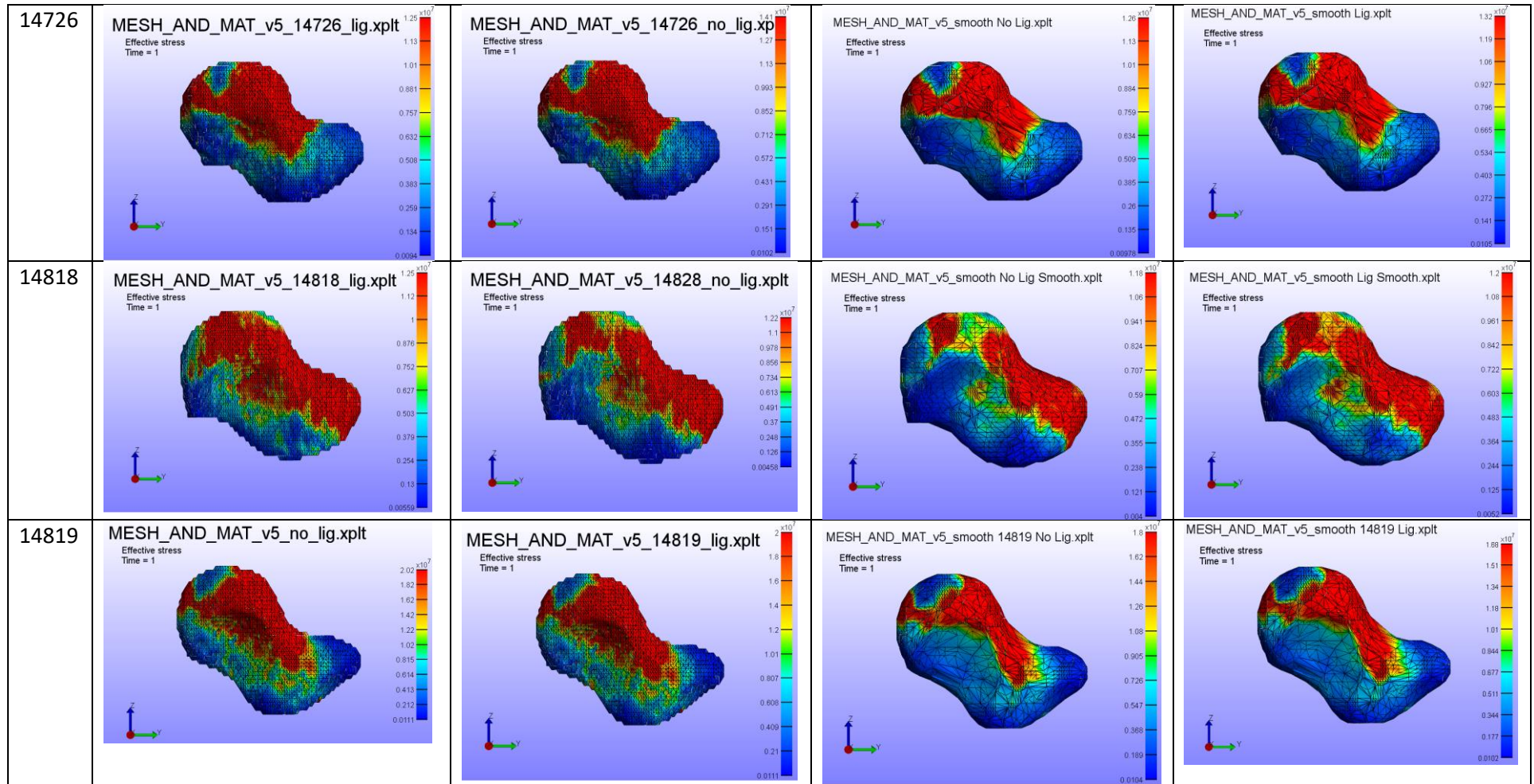
For mesh smoothing, the differences between data are significant, except for minimum strain for both ligament and no ligament simulations, and mean strain in simulations with no ligaments. Overall, there is statistical significance when smoothing the mesh in FE analysis using the methods in this project.

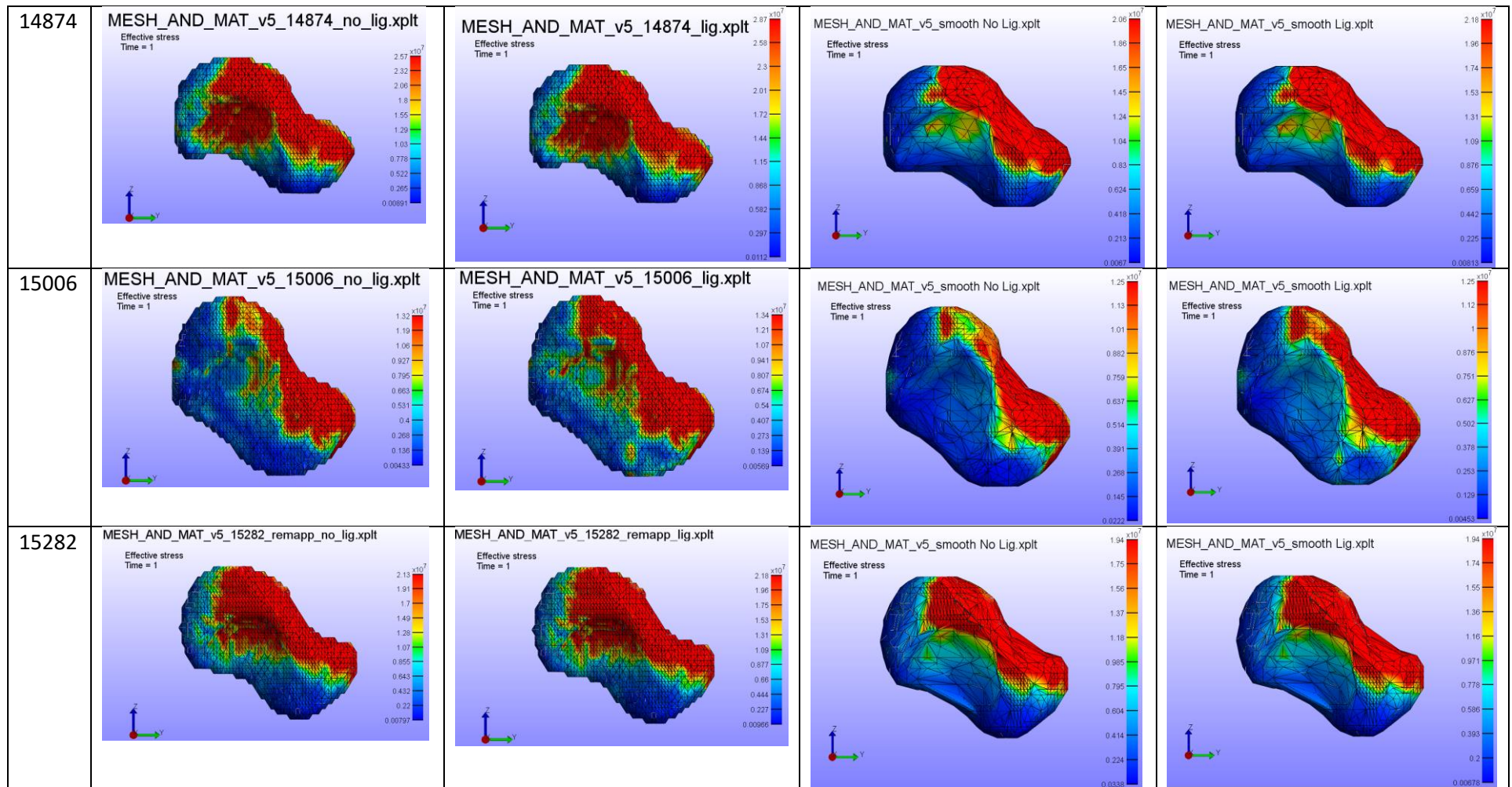
FE Analysis Results – Stress Distribution

Ulnar View

Table 11: Table containing FEBio screenshots of the stress heatmaps in the ulnar view of all simulations

Model	Unsmoothed		Smoothed	
	No Ligaments	Ligaments	No Ligaments	Ligaments
14548				
14613				

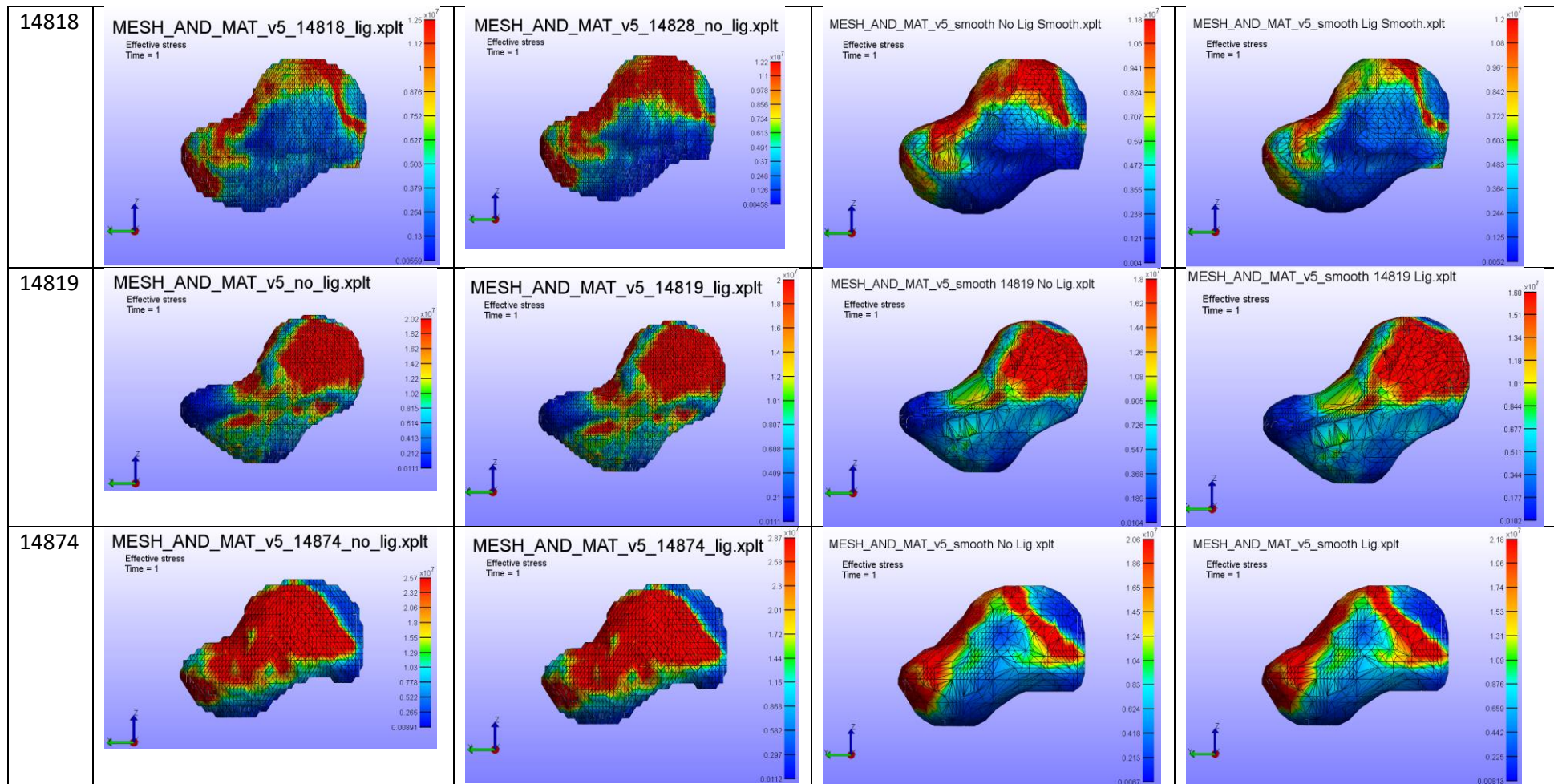


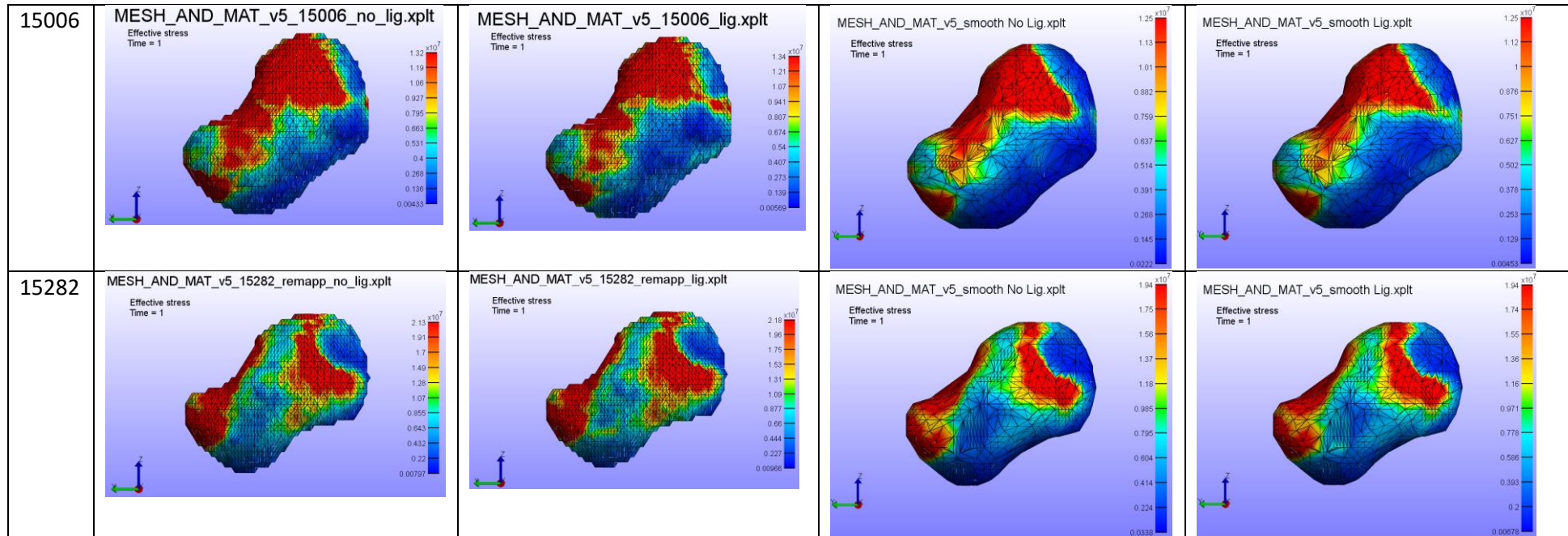


Radial View

Table 12: Table containing FEBio screenshots of the stress heatmaps in the radial view of all simulations

Model	Unsmoothed		Smoothed	
	No Ligaments	Ligaments	No Ligaments	Ligaments
14548	<p>MESH_AND_MAT_v5_14548_No_lig.xplt Effective stress Time = 1</p>	<p>MESH_AND_MAT_v5_14548_lig.xplt Effective stress Time = 1</p>	<p>MESH_AND_MAT_v5_smooth.xplt Effective stress Time = 1</p>	<p>MESH_AND_MAT_v5_smooth_lig.xplt Effective stress Time = 1</p>
14613	<p>MESH_AND_MAT_v5.xplt Effective stress Time = 1</p>	<p>MESH_AND_MAT_v5_with_Lig.xplt Effective stress Time = 1</p>	<p>MESH_AND_MAT_v5_smooth_No_lig.xplt Effective stress Time = 1</p>	<p>MESH_AND_MAT_v5_smooth_lig.xplt Effective stress Time = 1</p>
14726	<p>MESH_AND_MAT_v5_14726_lig.xplt Effective stress Time = 1</p>	<p>MESH_AND_MAT_v5_14726_no_lig.xp Effective stress Time = 1</p>	<p>MESH_AND_MAT_v5_smooth No Lig.xplt Effective stress Time = 1</p>	<p>MESH_AND_MAT_v5_smooth Lig.xplt Effective stress Time = 1</p>



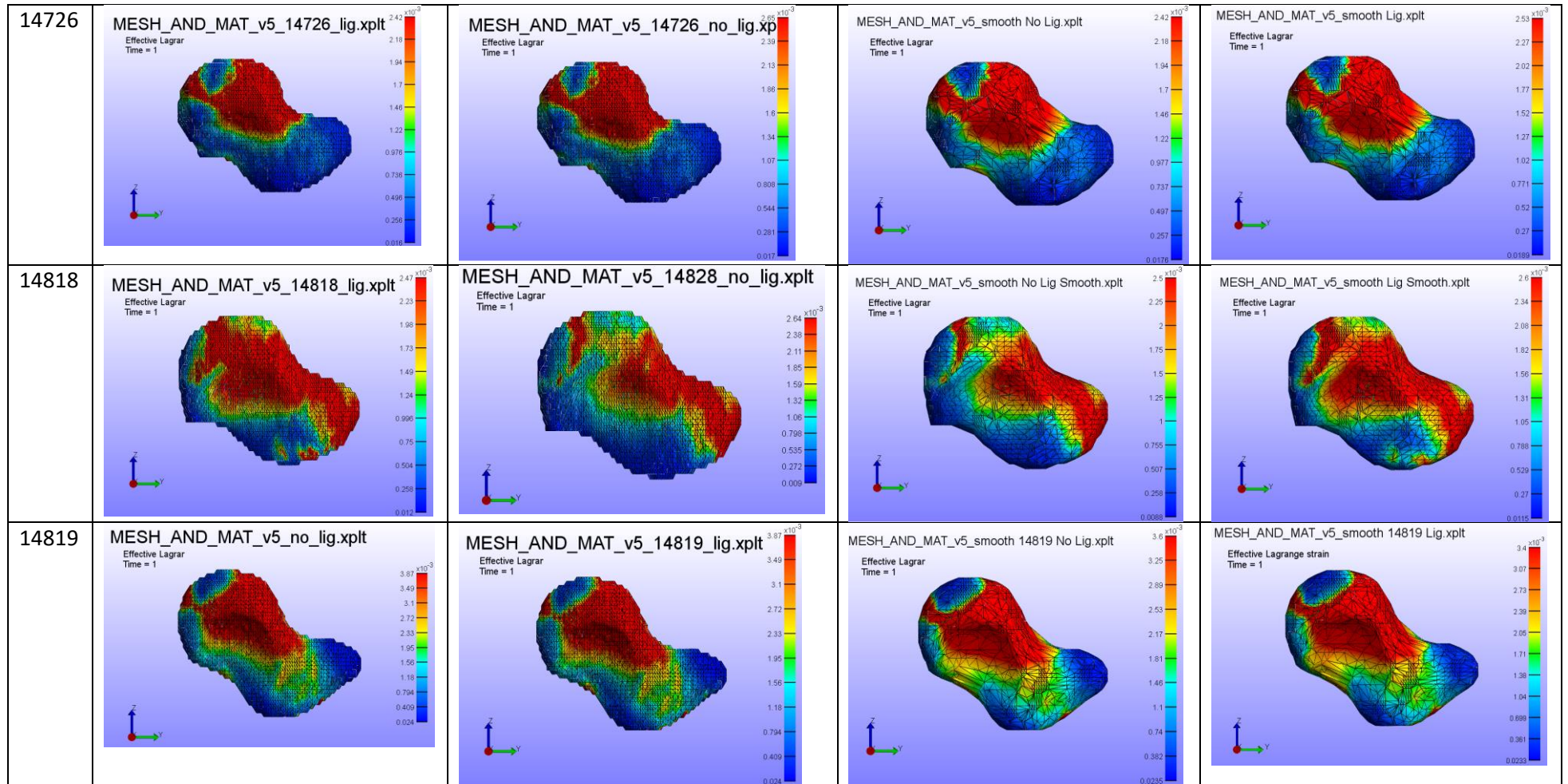


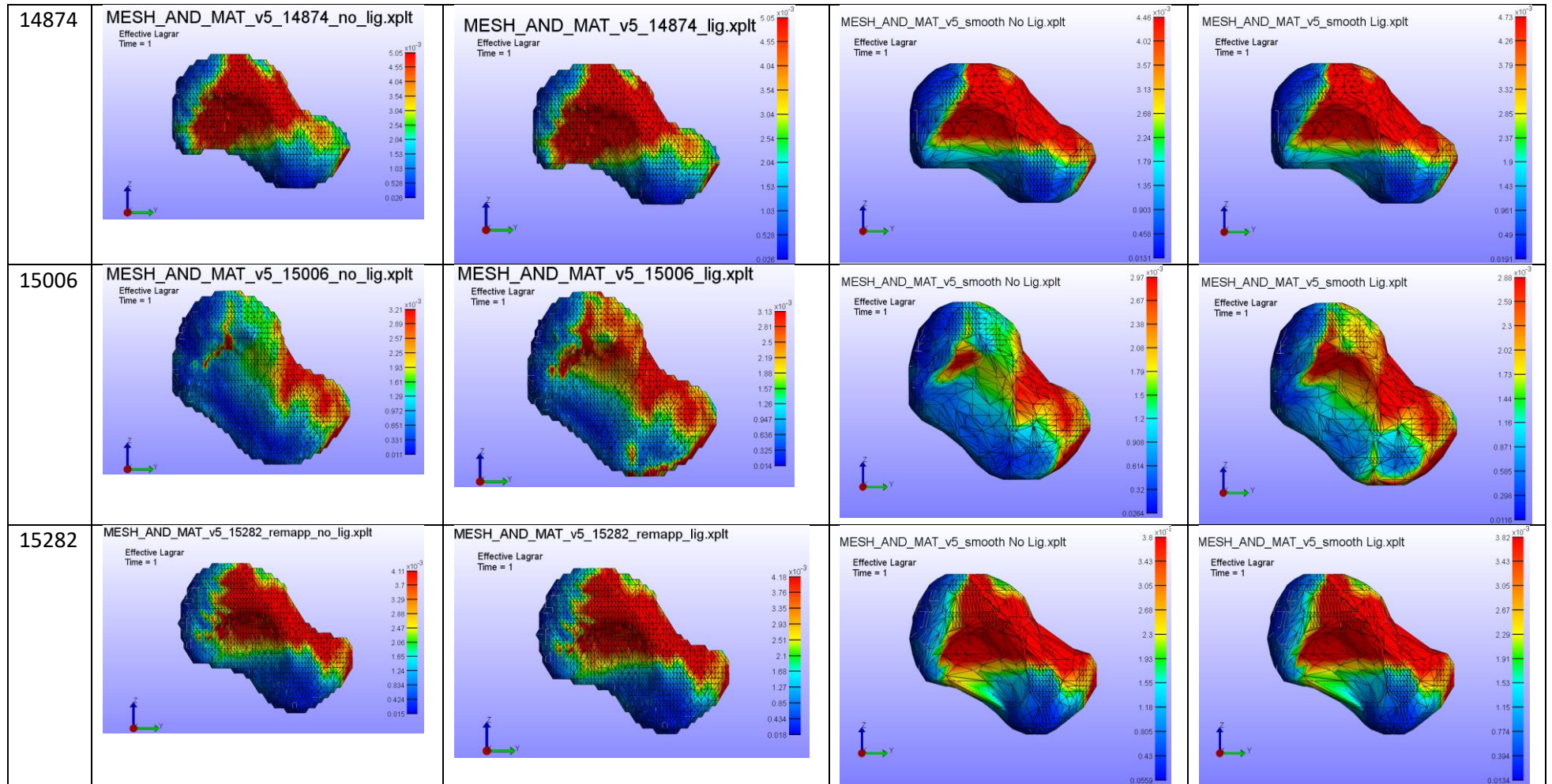
FE Analysis Results – Strain Distribution

Ulnar View

Table 13: Table containing FEBio screenshots of the strain heatmaps in the ulnar view of all simulations

Model	Unsmoothed		Smoothed	
	No Ligaments	Ligaments	No Ligaments	Ligaments
14548				
14613				

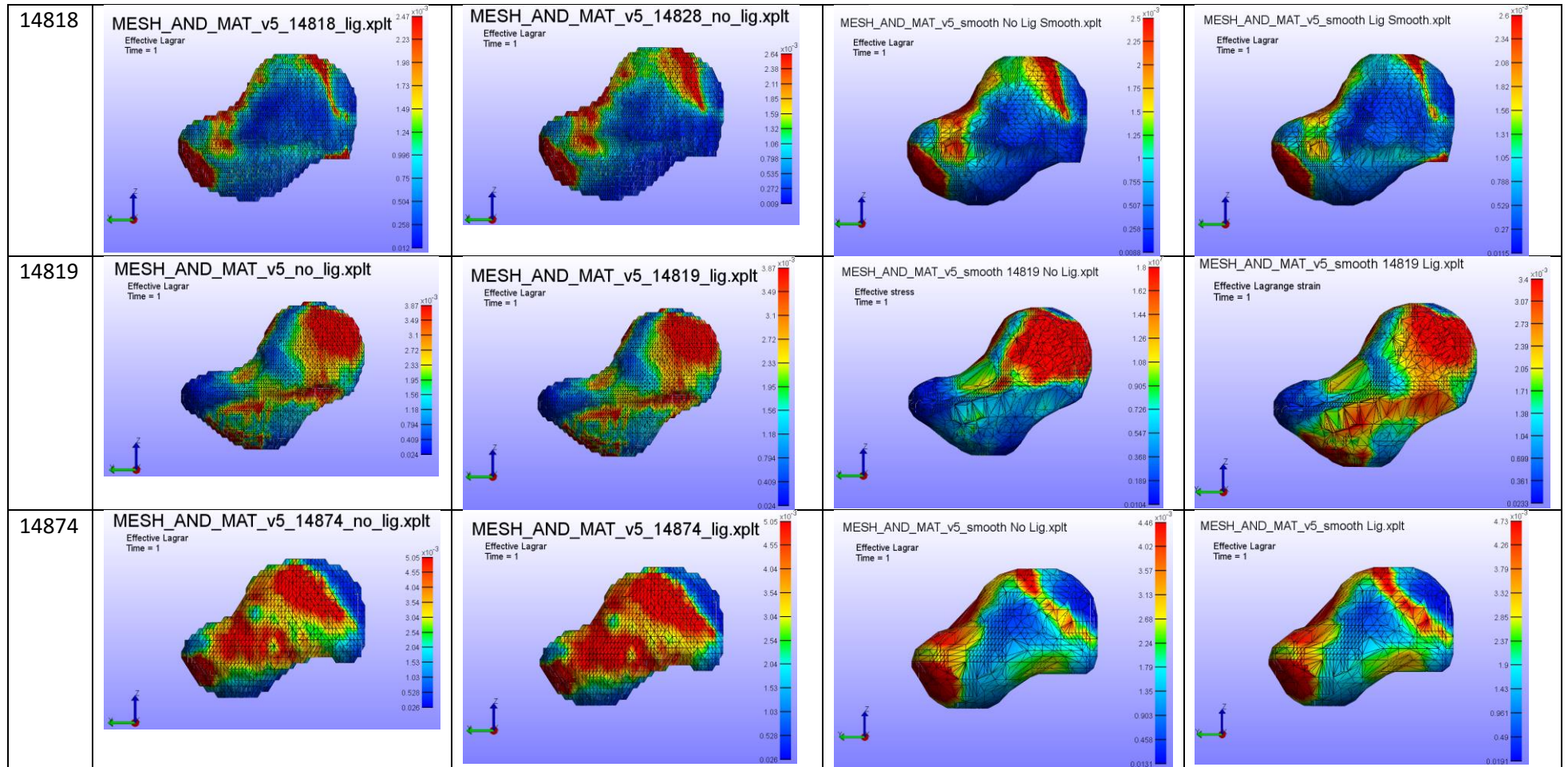


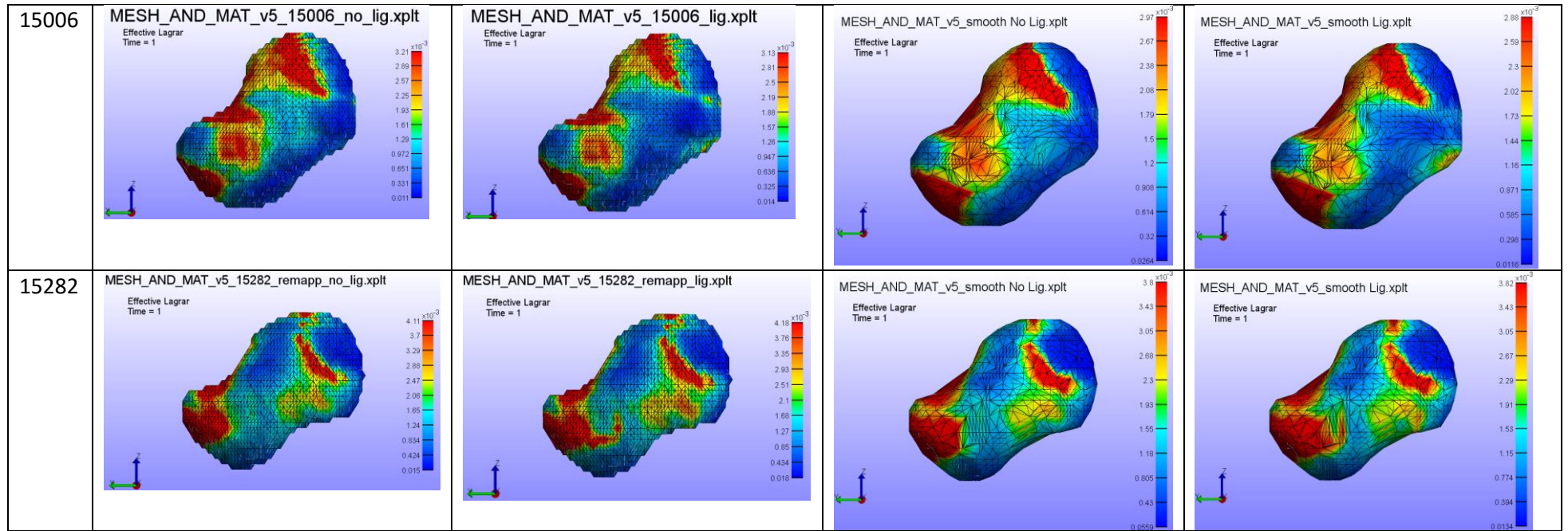


Radial View

Table 14: Table containing FEBio screenshots of the strain heatmaps in the radial view of all simulations

Model	Unsmoothed		Smoothed	
	No Ligaments	Ligaments	No Ligaments	Ligaments
14548				
14613				
14726				





Tables 11 to 14 show the stress and strain distributions of the finite element process after adjusting the heat map to represent the 95th and 5th percentiles. In all cases, the stress and strain patterns are similar for each model, however, the strain patterns tend to be less distributed. Another observation which can be made with strain distributions is improved consistency between smoothed and unsmoothed models. This is most easily noticed with models 14548 and 14613. In the ulnar view of the stress simulations, the simulations using the smoothed ligaments show a significant decrease in stresses around the proximal end of the dorsal side of the scaphoid. In contrast, the strain distributions are similar between the smoothed and unsmoothed simulations. This could represent strain simulations being less dependent on geometry compared to stress simulations.

In all scenarios, there are significant stress and strains occurring on the dorsal side of the scaphoid. In 6 cases, the stresses and strains are present from the proximal end to the distal end. In the remaining 2 cases, there are no significant stresses or strains at the distal end. The dorsal stresses and strains can travel radially or ulnarly and are positioned where the scaphoid capitate ligament would lie.

Model 14874 has the most significant variation in stress and strain distribution between smoothed and unsmoothed simulations in the radial view. The smoothed simulations show significant stresses around the proximal boundary condition, distal end and both ulnar and radial sides of the scaphoid. There are less significant stresses and strains at the radial face of the scaphoid. In contrast, in the unsmoothed model, there are significant stresses and strains occurring across the radial face of the scaphoid.

Table 9 and 10 showed there is a decrease in stress and strain across the scaphoid when smoothing the scaphoid by reducing the shrink factor in the MATLAB boundary function. The decrease between smoothing ligaments is smallest when comparing the maximum strain in scenarios with no ligaments (7.80% decrease) and largest when comparing the mean strain with no ligaments (25.36%). On average, there is a 14.07% (standard deviation: 5.14%) decrease in stresses and strains.

For the project, the scaphoids have significant variation in the number of elements (from ~70,000 to ~250,000). This represents a variation within the size of the scaphoid within the data set which needs to be addressed. As the size of the scaphoids can vary significantly, the effects of having varying scaphoid sizes with the same loading force must be analysed. The maximum FE predicted stress and strain values are compared to element count for each model in Figures 12 and 13.

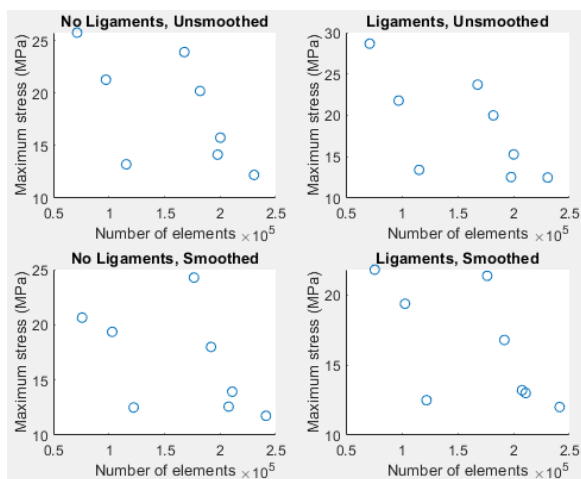


Figure 12: The four graphs show the change in maximum stress when increasing the mesh volume in all simulation types. There appears to be negative correlation.

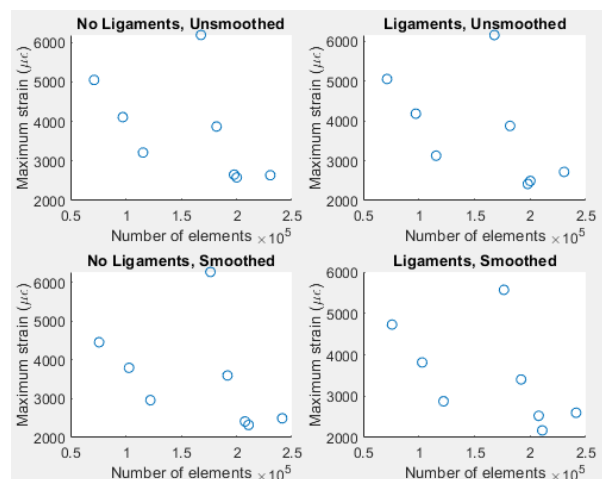


Figure 13: The four graphs show the change in maximum strain when increasing the mesh volume in all simulation types. There appears to be negative correlation.

Discussion

The FE analysis of the scaphoids show significant stresses and strains on the scaphoid in a simulated falling scenario where the loading force is 560N. The initial observation of the force distributions of the scaphoid shows significant stresses and strains around the proximal and sometime on the distal end of the scaphoid which are most likely boundary forces introduced in the finite element analysis step. By using the 95th and 5th percentiles, the boundary forces become less significant when observing the stress and strain distributions in the FE results. The analysis of the project found the most significant stresses in all scaphoids to occur on the dorsal side of the scaphoid. In some cases, significant stresses can occur at the proximal ulnar side of the scaphoid. In a falling scenario, these areas will be exposed to significant stresses and strains and would represent areas which are most likely to fracture. If the loading conditions are increased, propagation of the stress and strain distributions could be observed, and a scaphoid fracture propagation would be observed.

The second objective of the project is to analyse the effects of simulating ligament modelling on scaphoid biomechanics. In the unsmoothed and smoothed models, the most significant changes occur at the minimum (5th) stress and strains. In the unsmoothed simulations, the increase is 13.04% (minimum stress) and 11.02% (minimum strain). In the smoothed simulations, the increase is 11.4% (minimum stress) and 14.77% (minimum strain). Although these changes are significant, the minimum stresses and strains are at a level which are insignificant compared to the maximum finite element predicted stresses and strains. In addition, only the changes in minimum stress in unsmoothed ligaments is significant, whereas the minimum stress and strain in all other criteria are considered insignificant. Therefore, the simulation of ligaments is found to be insignificant in predicting fractures in scaphoids.

In mesh smoothing, there are significant decreases in stress and strain distributions across maximum, minimum and mean values. This decrease is supported numerically (decrease of between 7 to 25%) and statistically (all decreases are significant except for minimum strain in models with no ligaments). However, as the number of elements has increased due to the smoothing technique, the project can conclude that there is significant sensitivity to mesh geometry.

From figures 12 and 13 there is a negative correlation between predicted maximum stresses and strains and number of elements. Although the correlation is not very strong, this relationship is expected as the force remains constant for all simulations, whilst the scaphoid size is changing. A smaller model would be expected to have larger stresses and strains when loaded with the same loading conditions. Due to the method of smoothing the model, there is an increase of number of elements. Based on the figures 12 and 13, the increase in number of elements could also be cause of the decrease in stresses and strains observed in tables 9 and 10.

Another limitation to the current smoothing technique is the introduction of irregularities which can be found with element definitions. One example of this can be seen in model 15282 where an element is defined on the volar side of the scaphoid (Figure 14, blue arrow) which in unrealistic and is a direct result of the shrink factor decrease. Another irregularity can be seen on the surface of the models where there are sharp triangles (Figure 14, orange arrow) which can lead to high stress concentrations. To improve the smoothing process, there are alternative methods of smoothing which include the patchsmooth technique from GIBBON or the smoothpatch function (Dirk-Jan Kroon (2021)). These provide Laplacian and Humpfry's technique for smoothing of a surface mesh. The two mentioned functions to smooth the mesh are intended to smooth out a surface point cloud. In order to implement these into the project, the process of smoothing will have to be adjusted and will involve isolating the surface mesh, smoothing the surface and replacing corresponding nodes on

the scaphoid point cloud with smoothed surface point cloud nodes. As the smoothing analysis was performed late in the project, there was insufficient time to implement these changes and perform simulations again.

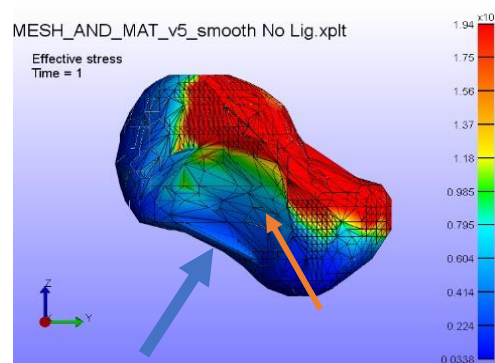


Figure 14: When using the current method of mesh smoothing, artifacts are created on the mesh surface which include irregular change to scaphoid shape (blue arrow and poor element shape).

The force distributions on the scaphoid can be comparable to the common fracture distributions mapped by A. Bulstra, et al. (2021). The results produced by Bulstra, et al. show common fracture lines tend to propagate between 20% and 80% on the volar side and dorsal ends where the percentage position represents the position of the fracture in relation to the proximal end of the scaphoid. In many simulations, the results show significant stresses and strains occurring around these positions on the dorsal side of the scaphoid (Example in Figure 14). Although the FE results do not show many significant stresses on the volar side, the results of the FE analysis are on the right track to producing more useful results. Currently, the results indicate the dorsal side of the scaphoid to be the location where the fracture is likely to initiate propagation due to having the most significant, non-boundary stress and strain distributions.

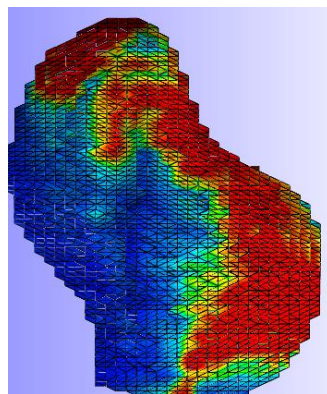


Figure removed due to copyright restriction

Figure 15: When using the current method of mesh smoothing, artifacts are created on the mesh surface which include irregular change to scaphoid shape (blue arrow and poor element shape) Comparison between stress distributions between Scaphoid 14818 and fracture lines described by Bulstra

Ivanmardian, et al. found that modelling of the ligaments may be insignificant in simulations of a grasping movement. The results of this project show that there are significant increases in minimum stress and strain. Although this the findings are significant, overall, for fracture and overall stress and strain predictions, the influence of ligaments is found to be quite small overall and insignificant overall which agrees with the finding of Ivanmardian.

In all models, the element size is based on the individual CT voxel size (0.3906mm x 0.3906mm) and scan thickness (0.6240 mm), therefore the element size is the smallest size which captures material property definitions with minimal extrapolation based on clinical scanning of scaphoids. However,

the mesh quality for the finite element analysis step was not evaluated. A higher density mesh will result in higher numerical analysis whilst increasing computation time. A mesh convergence study to find a mesh density which obtains theoretically accurate results that can be computed within a reasonable period of time. To perform a mesh convergence study, the mesh density must be changed for each step. For the project, the nodes are defined as locations of each voxel in a CT scan. To change the mesh density, more nodes must be created, and material properties must be mapped and associated to each new element. This process is relatively complex, and the implementation process is not very clear. There might be a function in ANSYS, however, further research and performing mesh convergence would have pushed the project past the time constraint.

Element definitions are 4 nodes tetrahedral (T4) elements. The T4 element type tends to be stiffer compared to the 8-noded hexahedral (H8) element and higher element types 10-noded tetrahedral (T10) and 20-noded hexahedral element (H20), leading to stress and strain values that are larger than the expected numerical results. To reduce the over-estimation associated with T4 elements, a smaller mesh size or a mesh size deemed appropriate based on the convergence study will improve FE estimations. Another solution would be to implement a higher order element type with the same mesh density; however, this will require interpolation of material property definitions. Various papers have demonstrated the use of H8 elements such the papers produced by L. Cyganik, et al., S. Kazembakhski, Y. Luo, and W. Enns-Bray, et al. These papers converted individual voxels to H8 elements using various algorithms and constrained the surface of the FE model to a microCT scanned model.

Due to the lack of numerical results from the same specimens as the model and mesh convergence, there is no method of determining the influence of the use of T4 elements on the FE solutions. Peak stresses and strains derived from the results of the FE results of the project are unlikely to be usable as fracture predictors. With that being said, the stress and strain distributions can be used as regions of high stress and strains, which can be used as indicators for regions of fracture initiation. To avoid the limitations of using T4 elements, H8 elements should be used for future simulations. One paper performed preliminary research on stress and strain predictions in a scaphoid fracture scenario and found fracturing to occur at forces around 1204.3N with a peak stress of 2.64 MPa, when loaded at a rate of 700mm/min (R. Kiss, 2020). In contrast, the force used in this project was around 560N and found the average peak stress (95th percentile) to be around 17 MPa. The fracture criteria for the paper was 2mm displacement. As the displacement was not analysed in this project, the significant difference (larger fracture load and peak stress found by R. Kiss) may be due to applying a strain rate load rather than a set load.

The models of the scaphoid in this project assumes the same relationship between material properties and Hounsfield units can be used for all nodes of the model. This is unlikely to be the case as cortical and trabecular bone are likely to have different material property relationships. Morgan, et al. (2003) was able to demonstrate there is no relationship which can relate density to Young's modulus of elasticity for trabecular bone across all anatomic sites. Different relationships between material property with density will have different ranges at which the relationships are reliable (E. Morgan, 2003). As such, using a single density to material property definition for the scaphoid could result in inaccurate results. The project assumed a relationship for cortical bone for all nodes, thus, the trabecular bone within the scaphoid would be overestimated, thus increased load bearing of the trabecular bone, leading to less accurate stress and strain distributions.

Miura, et al. (2017) Verified and defined material property definitions / calibrations for each specimen through comparison on predicted material properties and experimental determination of material properties. For this project, the same relationship was used for all models, assuming the

calibration of all models was the same, all bones were healthy and the same relationship can be applied to all specimens. If the HU units were calibrated differently between scans, the relationship between HU and material properties will be different for each model, thus model / specimen specific material property definitions are necessary. To validate material property definitions, a sample must be extracted from the patient. As the models are from CT scans of scaphoids within healthy subjects, extracting a sample for material property evaluation would be difficult to obtain. Although material property validation is important, the validation process will be difficult to perform in healthy patients.

Another assumption which was made for all elements is the isotropic material property definitions. Bone, especially trabecular bone, is highly anisotropic, thus defining anisotropic relationships for all elements would create more accurate models. To perform this, microCT is necessary to determine bone primary anisotropic directions which is incorporated into the model. Although the accuracy would be improved, computation time is significantly increased, which could be undesirable. Synek, et al. (2015), found that modelling anisotropic material properties in femoral FE analysis did not significantly improve results. Synek, et al. (2015) also found that inhomogeneous material properties were significant within the proximal femur. The project implemented an isotropic, inhomogeneous material property definitions, which will produce reliable results as the modelling of anisotropy will not lead to improved results.

In the finite element modelling process, the radioscapoid joint mapping may not be physiologically accurate. The error is due to the misinterpretation of literature data. The mapping of the joint contact area should be more dorsal and can be fixed by adjusting the mapping definitions. The incorrect mapping of the boundary condition has likely influenced the result of the FE analysis. If the boundary condition was moved more dorsally to be more similar with literature, the force due to falling is more likely to create bending moments throughout the scaphoid, which will create different stress and strain patterns. Mastuura, et al. (2017), modelled the wrist observe forces throughout the wrist in falling scenarios which lead to Smith's fractures. Iavanmardian, et al. (2010) modelled the wrist to compare the effects of simulating ligaments within the wrist connecting to the radius and ulnar with simulations without ligaments. By modelling the whole wrist, the contact between carpal bones and radius can be determined using FE analysis whereas this project assumed there is no contact between carpal bones and predicts contact based on literature. The significance of this assumption cannot be validated based on literature or numerical results.

The force due to falling is assumed to be acting on the distal scaphoid at an estimated contact area. There is little to no literature which describes the forces or area of application of the force. As a result, the falling force is assumed to be perpendicular to the surface. This is unlikely to be the case as Mastuura, et al. (2017), found scaphoid fracturing can occur when falling onto the hand where the arm is at an angle where the radius is angled non-perpendicularly to the ground. The force is unlikely to be acting perpendicular to the surface of the scaphoid and can lead to significant bending forces and create more fracture like stress and strain distributions. Few or no previous papers have attempted to simulate falling onto the scaphoid without simulating the whole wrist. Further research is needed to determine the direction and area of loading on the scaphoid in a falling scenario to improve the assumptions related to scaphoid loading.

The magnitude of the force due to falling is also assumed to be 70% of an assumed body weight of 800N (total of 560N). This is an assumption which had to be made as there is no literature regarding how much force is applied to the scaphoid in a falling scenario. Majima, et al. (2007), was able to determine that approximately 52 – 64% of the force applied onto the wrist will be transferred through the scaphoid in an extended position. No literature was found on the total load on the wrist

in a falling scenario, however, Lee (2019), stated that using a percentage of body weight would be more accurate compared to using a set force in all scenarios. A constant force acting on each of the scaphoid is unrealistic due to the natural variation in scaphoid shape and sizes, this a constant force would not reliably replicate the true force the specific scaphoid undergoes. To improve this project, further research is needed to determine the magnitude of falling force in relation to the body weight of the patient. It may be possible to find correlation between the size of the scaphoid and load the scaphoid will be exposed to in a falling scenario.

The assumption for the contact area was any nodes within a certain radius of the estimated centroid, therefore the contact area is assumed to be circular. In literature, the contact area is not circular and is irregular. Due to the complexity of the contact area and lack of ability to directly map the contact area onto the statistical scaphoid model, the simplest and easiest method of mapping the contact area is to use the circular assumption mentioned.

The influence of ligaments is assumed to be the same for all ligaments (20N perpendicular tensile force). This is unlikely to be true as ligaments have different functionality and do not all act in a perpendicular tensile direction. Due to a lack of literature describing the forces due to ligaments in a falling scenario, a force of 20N is assumed for all ligaments. Dimitris, et al. (2010), and Scordino (2017), were able to determine that the SLIL produces 20N of force in cyclic motion and 44.5N in a push up position. These forces are produced in natural movement within a human wrist. As a result, a 20N force produced by each ligament in a falling scenario is highly unlikely to be realistic. The true force would be larger than 20N. To produce more accurate results when ligaments are mapped, further research is needed in direction and magnitude of ligament forces. However, Iavanmardian, et al. (2010), proposes that ligaments do not play a significant role in FE results, thus improving ligament accuracy may be unnecessary.

The ligament attachment areas are mapped onto the statistical model based on literature by G. Buijze, et al., 2011, and Y. Kijima, et al., 2009. Although this should provide a good method of mapping the ligaments onto each scaphoid, the mapping may not be representative of the actual ligament mapping on each individual scaphoid. Y. Kijima, et al., 2009 has shown that there is variation in some ligament presence and attachment coverage area. Alongside this specimen-to-specimen variation, all ligaments are assumed to be healthy, thus, if the ligaments exist, the influence of the ligament will be consistent for all specimens. This would not be true for all specimens, especially the specimens with SLIL injuries. The SLIL is the most significant scaphoid lunate stabiliser and when this is damaged, the scaphotrapezoidal ligament and scaphotrapezium ligament become more significant. The current mapping technique does not take ligament damage or presence into consideration and would not be the most accurate technique for mapping ligaments. Based on the findings of the project, the simulations of ligaments were found to be insignificant, therefore, ligament inconsistencies are unlikely to have significantly influenced the results.

The project aims to be able to predict stress and strain distributions throughout the scaphoid when modelling only the scaphoid with forces representative of the forces the scaphoid is exposed to in the wrist. From literature, this has not been done previously as other papers have modelled the wrist for FE analysis.

Although the objective for this project is to determine stress and strain distributions on the scaphoid in a simulated falling scenario, it would be beneficial to determine a fracture line. Determining the definition of a fracture is difficult as there are various methods to determine what is a fracture. Lee (2019), reviewed definitions of fractures of various papers and found various definitions for fracture.

Fracture can be defined as when the predicted stress exceeds the predicted material strength of the material (Keyak). In addition to these definitions, fracture can also be defined as straining at different thresholds or number of failed elements. To define a fracture line for this project, a definite fracture definition based on literature and reasonable assumptions must be made.

Future work

To improve the stress and strain predictions on the scaphoid in a falling scenario, the loading and boundary conditions need to be better defined. The current radioscapoid joint is modelled as a circle based on a centroid position. The centroid position is in the wrong position and the radioscapoid joint is not a circular contact area. To improve the radioscapoid joint, there needs to be a better method to define the irregular shape of the contact surface, such as using computer algorithms to map an experimentally determined joint contact area onto a scaphoid, then using multiple non-rigid-ICP iterations to map to a scaphoid model.

In terms of loading conditions, the vector definitions for both the ligaments and falling force needs to be better defined. Currently, both forces are assumed to be perpendicular to the scaphoid face when, the forces are likely to be acting at some angle to the surface. To improve the vector definitions, further research must be made in terms of determining the direction the falling force acts on the scaphoid, how large the falling force is and ligament force and direction on the scaphoid. Better defining ligament direction can be performed in conjunction with Flinders medical students and Prof. Greg Bain who are willing to investigate ligament directionality using cadavers.

As mentioned in the discussion, a better method of mesh smoothing must be used to improve the conclusions made regarding mesh smoothing. Patchsmooth and Smoothpatch can be implemented in MATLAB to use Humfry and/or Laplacian smoothing on the surface nodes to adjust nodal positions rather than creating more element definitions.

On key step that was missed in the FE mesh creation was a mesh convergence study. For all models, the element sizes were kept constant, based on the voxel size of the CT scan slices. Although using the same element size reduces the interpolation of material properties, the mesh density varies significantly between models. Future work of this scaphoid modelling will require a mesh convergency study to reduce the influence of the use of T4 elements in FEA.

Conclusion

The project could perform finite element analysis of the scaphoid in a falling scenario. In all simulation, the most significant stresses and strains occur on the dorsal side of the scaphoid between the apex and proximal boundary conditions. In all simulations, the same force was applied to all models, therefore, the accuracy and real-life representations of the stress and strain distributions are unusable. Due to the varying scaphoid volumes between models, smaller models will have larger stress and strain predictions. As a result, the current stress and strain patterns are an indicator that FE analysis of the scaphoid can be done, however, the loading conditions need to be improved to obtain better real-life indicators on stress and strain distributions and possible fracture line predictions using FEA of a scaphoid model.

Simulating ligament was found to have a significant affect on the minimum stresses and strain (5th percentile values) values in all FE simulations, however, the minimum stresses and strains are unlikely to have significant impacts on overall stresses and strains on the scaphoid, therefore, ligament simulation is considered to have minimal impact on the overall simulations.

From the FE analysis, smoothing the mesh resulted in a significant decrease in stresses and strains across the entire distribution (5th percentile, average and 95th percentile). It could be concluded that smoothing the meshes had a profound effect on reducing the stress concentrations of the non-smoothed model, however, due to an increase in number of elements (associated with increase in volume, not element density), the true influence of smoothing the model must be further researched.

References

1. Akram, S. and Chowdhury, Y., 2020. *StatPearls [Internet]*.. Treasure Island (FL): StatPearls Publishing.
2. Bäcker, H., Wu, C. and Strauch, R., 2019. Systematic Review of Diagnosis of Clinically Suspected Scaphoid Fractures. *Journal of Wrist Surgery*, 09(01), pp.081-089.
3. Buijze, G., Dvinskikh, N., Strackee, S., Streekstra, G. and Blankevoort, L., 2011. Osseous and Ligamentous Scaphoid Anatomy: Part II. Evaluation of Ligament Morphology Using Three-Dimensional Anatomical Imaging. *The Journal of Hand Surgery*, 36(12), pp.1936-1943.
4. Bulstra, A., Al-Dirini, R., Turow, A., Oldhoff, M., Bryant, K., Obdeijn, M., Doornberg, J., Jaarsma, R. and Bain, G., 2021. The influence of fracture location and comminution on acute scaphoid fracture displacement: three-dimensional CT analysis. *Journal of Hand Surgery (European Volume)*, p.175319342110409.
5. Cheema, A., Niziolek, P., Steinberg, D., Kneeland, B., Kazmers, N. and Bozentka, D., 2018. The Effect of Computed Tomography Scans Oriented Along the Longitudinal Scaphoid Axis on Measurements of Deformity and Displacement in Scaphoid Fractures. *The Journal of Hand Surgery*, 43(12), pp.1092-1097.
6. Chen, Y., Wu, Y., Tang, J. and Giddins, G., 2013. Contact areas of the scaphoid and lunate with the distal radius in neutral and extension: correlation of falling strategies and distal radial anatomy. *Journal of Hand Surgery (European Volume)*, 39(4), pp.379-383.
7. Cyganik, Ł., Binkowski, M., Kokot, G., Cyganik, P., Rusin, T., Bolechała, F., Nowak, R., Wróbel, Z. and John, A., 2017. Microscale's relationship between Young's modulus and tissue density. Prediction of displacements. *Computer Methods in Biomechanics and Biomedical Engineering*, 20(16), pp.1658-1668.
8. Cyganik, Ł., Binkowski, M., Kokot, G., Rusin, T., Popik, P., Bolechała, F., Nowak, R., Wróbel, Z. and John, A., 2014. Prediction of Young's modulus of trabeculae in microscale using macro-scale's relationships between bone density and mechanical properties. *Journal of the Mechanical Behavior of Biomedical Materials*, 36, pp.120-134.
9. Dan Couture (2021). Plane Fitting and Normal Calculation (<https://www.mathworks.com/matlabcentral/fileexchange/37775-plane-fitting-and-normal-calculation>), MATLAB Central File Exchange. Retrieved October 27, 2021.
10. de Bakker, C., Tseng, W., Li, Y., Zhao, H. and Liu, X., 2017. Clinical Evaluation of Bone Strength and Fracture Risk. *Current Osteoporosis Reports*, 15(1), pp.32-42.
11. Dimitris, C., Werner, F., Joyce, D. and Harley, B., 2015. Force in the Scapholunate Interosseous Ligament During Active Wrist Motion. *The Journal of Hand Surgery*, 40(8), pp.1525-1533.
12. Dirk-Jan Kroon (2021). Smooth Triangulated Mesh (<https://www.mathworks.com/matlabcentral/fileexchange/26710-smooth-triangulated-mesh>), MATLAB Central File Exchange. Retrieved October 27, 2021.
13. Enns-Bray, W., Owoc, J., Nishiyama, K. and Boyd, S., 2014. Mapping anisotropy of the proximal femur for enhanced image based finite element analysis. *Journal of Biomechanics*, 47(13), pp.3272-3278.
14. Faragó, D. and Kiss, R., 2020. Geometric and Mechanical Characterization of Human Carpal Bones – a Preliminary Study. *Periodica Polytechnica Civil Engineering*,.

15. Fleps, I., Bahaloo, H., Zysset, P., Ferguson, S., Pálsson, H. and Helgason, B., 2020. Empirical relationships between bone density and ultimate strength: A literature review. *Journal of the Mechanical Behavior of Biomedical Materials*, 110, p.103866.
16. Garala, K. and Dias, J., 2019. Scaphoid fracture geometrics: an assessment of location and orientation. *Journal of Plastic Surgery and Hand Surgery*, 53(3), pp.180-187.
17. Grassi, L., Schileo, E., Boichon, C., Viceconti, M. and Taddei, F., 2014. Comprehensive evaluation of PCA-based finite element modelling of the human femur. *Medical Engineering & Physics*, 36(10), pp.1246-1252.
18. Gujar, R. and Warhatkar, H., 2020. Estimation of mass apparent density and Young's modulus of femoral neck-head region. *Journal of Medical Engineering & Technology*, 44(7), pp.378-388.
19. Hambli, R., Bettamer, A. and Allaoui, S., 2012. Finite element prediction of proximal femur fracture pattern based on orthotropic behaviour law coupled to quasi-brittle damage. *Medical Engineering & Physics*, 34(2), pp.202-210.
20. Holmes, M., Howarth, S., Callaghan, J. and Keir, P., 2011. Carpal tunnel and transverse carpal ligament stiffness with changes in wrist posture and indenter size. *Journal of Orthopaedic Research*, 29(11), pp.1682-1687.
21. Jaadi, Z., 2021. A Step-by-Step Explanation of Principal Component Analysis (PCA). [online] Built In. Available at: <<https://builtin.com/data-science/step-step-explanation-principal-component-analysis>> [Accessed 22 October 2021].
22. Kazembakhshi, S. and Luo, Y., 2014. Constructing anisotropic finite element model of bone from computed tomography (CT). *Bio-Medical Materials and Engineering*, 24(6), pp.2619-2626.
23. Kijima, Y. and Viegas, S., 2009. Wrist Anatomy and Biomechanics. *The Journal of Hand Surgery*, 34(8), pp.1555-1563.
24. KUHLMANN, J., LUBOINSKI, J., LAUDET, C., BOABIGHI, A., LANDJERIT, B., GUERINSURVILLE, H. and BAUX, S., 1990. Properties of the fibrous structures of the wrist. *The Journal of Hand Surgery: Journal of the British Society for Surgery of the Hand*, 15(3), pp.335-341.
25. Lee, Y., Ogihara, N. and Lee, T., 2019. Assessment of finite element models for prediction of osteoporotic fracture. *Journal of the Mechanical Behavior of Biomedical Materials*, 97, pp.312-320.
26. Mack, M., Keim, S., Balzer, J., Schwarz, W., Hochmuth, K., Windolf, J. and Vogl, T., 2003. Clinical impact of MRI in acute wrist fractures. *European Radiology*, 13(3), pp.612-617.
27. MacNeil, J. and Boyd, S., 2007. Load distribution and the predictive power of morphological indices in the distal radius and tibia by high resolution peripheral quantitative computed tomography. *Bone*, 41(1), pp.129-137.
28. Majima, M., Horii, E., Matsuki, H., Hirata, H. and Genda, E., 2008. Load Transmission Through the Wrist in the Extended Position. *The Journal of Hand Surgery*, 33(2), pp.182-188.
29. Mallee, W., Walenkamp, M., Mulders, M., Goslings, J. and Schep, N., 2020. Detecting scaphoid fractures in wrist injury: a clinical decision rule. *Archives of Orthopaedic and Trauma Surgery*, 140(4), pp.575-581.

30. Martelli, S. and Perilli, E., 2018. Time-elapsd synchrotron-light microstructural imaging of femoral neck fracture. *Journal of the Mechanical Behavior of Biomedical Materials*, 84, pp.265-272.
31. Matsuura, Y., Rokkaku, T., Kuniyoshi, K., Takahashi, K., Suzuki, T., Kanazuka, A., Akasaka, T., Hirose, N., Iwase, M., Yamazaki, A., Orita, S. and Ohtori, S., 2017. Smith's fracture generally occurs after falling on the palm of the hand. *Journal of Orthopaedic Research*, 35(11), pp.2435-2441.
32. Miura, M., Nakamura, J., Matsuura, Y., Wako, Y., Suzuki, T., Hagiwara, S., Orita, S., Inage, K., Kawarai, Y., Sugano, M., Nawata, K. and Ohtori, S., 2017. Prediction of fracture load and stiffness of the proximal femur by CT-based specimen specific finite element analysis: cadaveric validation study. *BMC Musculoskeletal Disorders*, 18(1).
33. Moerman, Kevin M. "GIBBON: The Geometry and Image-Based Bioengineering Add-On." *The Journal of Open Source Software*, vol. 3, no. 22, The Open Journal, Feb. 2018, p. 506, doi:10.21105/joss.00506.
34. Morgan, E., Bayraktar, H. and Keaveny, T., 2003. Trabecular bone modulus–density relationships depend on anatomic site. *Journal of Biomechanics*, 36(7), pp.897-904.
35. Nagao, S., Patterson, R., Buford, W., Andersen, C., Shah, M. and Viegas, S., 2005. Three-Dimensional Description of Ligamentous Attachments Around the Lunate. *The Journal of Hand Surgery*, 30(4), pp.685-692.
36. Nanno, M., Buford, W., Patterson, R., Andersen, C. and Viegas, S., 2006. Three-Dimensional Analysis of the Ligamentous Attachments of the First Carpometacarpal Joint. *The Journal of Hand Surgery*, 31(7), pp.1160-1170.
37. Nanno, M., Buford, W., Patterson, R., Andersen, C. and Viegas, S., 2007. Three-dimensional analysis of the ligamentous attachments of the second through fifth carpometacarpal joints. *Clinical Anatomy*, 20(5), pp.530-544.
38. Nerot, A., Skalli, W. and Wang, X., 2016. A principal component analysis of the relationship between the external body shape and internal skeleton for the upper body. *Journal of Biomechanics*, 49(14), pp.3415-3422.
39. Nikolopoulos, F., Apergis, E., Poulilios, A., Papagelopoulos, P., Zoubos, A. and Kefalas, V., 2011. Biomechanical properties of the scapholunate ligament and the importance of its portions in the capitate intrusion injury. *Clinical Biomechanics*, 26(8), pp.819-823.
40. Polgar, K., Gill, H., Viceconti, M., Murray, D. and O'Connor, J., 2003. Strain distribution within the human femur due to physiological and simplified loading: Finite element analysis using the muscle standardized femur model. *Proceedings of the Institution of Mechanical Engineers, Part H: Journal of Engineering in Medicine*, 217(3), pp.173-189.
41. Rhemrev, S., Ootes, D., Beeres, F., Meylaerts, S. and Schipper, I., 2011. Current methods of diagnosis and treatment of scaphoid fractures. *International Journal of Emergency Medicine*, 4(1).
42. Scordino, L., Werner, F. and Harley, B., 2016. Force in the Scapholunate Interosseous Ligament During 2 Simulated Pushup Positions. *The Journal of Hand Surgery*, 41(5), pp.624-629.
43. Sendher, R. and Ladd, A., 2013. The Scaphoid. *Orthopedic Clinics of North America*, 44(1), pp.107 - 120.

44. Short, W., Werner, F., Green, J., Sutton, L. and Brutus, J., 2007. Biomechanical Evaluation of the Ligamentous Stabilizers of the Scaphoid and Lunate: Part III. *The Journal of Hand Surgery*, 32(3), pp.297.e1-297.e18.
45. Sudhyadhom, A., 2020. On the molecular relationship between Hounsfield Unit (HU), mass density, and electron density in computed tomography (CT). *PLOS ONE*, 15(12), p.e0244861.
46. Synek, A., Chevalier, Y., Baumbach, S. and Pahr, D., 2015. The influence of bone density and anisotropy in finite element models of distal radius fracture osteosynthesis: Evaluations and comparison to experiments. *Journal of Biomechanics*, 48(15), pp.4116-4123.
47. Taddei, F., Martelli, S., Reggiani, B., Cristofolini, L. and Viceconti, M., 2006. Finite-Element Modeling of Bones From CT Data: Sensitivity to Geometry and Material Uncertainties. *IEEE Transactions on Biomedical Engineering*, 53(11), pp.2194-2200.
48. Tang, J. and Chen, Y., 2012. In Vivo Changes in Contact Regions of the Radiocarpal Joint During Wrist Hyperextension. *The Journal of Hand Surgery*, 37(11), pp.2257-2262.
49. Turner, C., Rho, J., Takano, Y., Tsui, T. and Pharr, G., 1999. The elastic properties of trabecular and cortical bone tissues are similar: results from two microscopic measurement techniques. *Journal of Biomechanics*, 32(4), pp.437-441.
50. Turow, A., Bulstra, A., Oldhoff, M., Hayat, B., Doornberg, J., White, J., Jaarsma, R. and Bain, G., 2020. 3D mapping of scaphoid fractures and comminution. *Skeletal Radiology*, 49(10), pp.1633-1647.
51. van de Giessen, M., Foumani, M., Streekstra, G., Strackee, S., Maas, M., van Vliet, L., Grimbergen, K. and Vos, F., 2010. Statistical descriptions of scaphoid and lunate bone shapes. *Journal of Biomechanics*, 43(8), pp.1463-1469.
52. Varga, P., Schefzig, P., Unger, E., Mayr, W., Zysset, P. and Erhart, J., 2013. Finite element based estimation of contact areas and pressures of the human scaphoid in various functional positions of the hand. *Journal of Biomechanics*, 46(5), pp.984-990.
53. Varga, P., Zysset, P., Schefzig, P., Unger, E., Mayr, W. and Erhart, J., 2016. A finite element analysis of two novel screw designs for scaphoid waist fractures. *Medical Engineering & Physics*, 38(2), pp.131-139.
54. Viegas, S., Yamaguchi, S., Boyd, N. and Patterson, R., 1999. The dorsal ligaments of the wrist: Anatomy, mechanical properties, and function. *The Journal of Hand Surgery*, 24(3), pp.456-468.
55. Vivanco, J., Burgers, T., García-Rodríguez, S., Crookshank, M., Kunz, M., MacIntyre, N., Harrison, M., Bryant, J., Sellens, R. and Ploeg, H., 2014. Estimating the density of femoral head trabecular bone from hip fracture patients using computed tomography scan data. *Proceedings of the Institution of Mechanical Engineers, Part H: Journal of Engineering in Medicine*, 228(6), pp.616-626.

Appendix: Core MATLAB Program

```
clear
clc
close all
model = '14548';
mat_file_path = ['F:\Master Thesis\Data from Brown\', model, '\Models'];
mat_file = 'sca_cropped.mat';
bone_threshold = 50;
load([mat_file_path, '\', mat_file]);

xPixel = ref_Small.PixelExtentInWorldX;
yPixel = ref_Small.PixelExtentInWorldY;
zPixel = ref_Small.PixelExtentInWorldZ;

Coords = [];
HU_values = [];

A = NIn(:, :, :);

A(A < bone_threshold) = 0;
A(A >= bone_threshold) = 255;
%%Matrix of non zero elements
nonZeroElements = A ~= 0;

for i = 1:size(A,1)
    for j = 1:size(A,2)
        for k = 1:size(A,3)
            if A(i,j,k) ~= 0
                Coords = [Coords; [i*xPixel, j*yPixel, k*zPixel]];
                HU_values = [HU_values; NIn(i, j, k)];
                %%
                A2(i, j, k) = 255;
                %%
            else
                %%
                A2(i, j, k) = 0;
                %%
            end
        end
    end
end

%%
a = 1.84675675675676e-01;
a = 0;
b = (((1.7-1e-3)/double(max(reshape(NIn, [], 1)) - min(reshape(NIn, [], 1)))));
rho = a + b*double(HU_values);
rho(rho<=0) = 0.00001;
E = 14664.*rho.^1.49; % -- morgan // modulus for each node MPA

connectivity = boundary(Coords, 0.99);

mesh2.vertices = Coords;
mesh2.faces = connectivity;

%%DelaunayTriangulation of Coords
% DT = delaunayTriangulation(Coords); %%DT.Points = nodal positions,
DP.ConnectivityList = nodes per element
DT = constrainedDelaunayTetGen(mesh2.vertices, mesh2.faces); %GIBBON
```

```

%%Find average Young's Modulus of Elasticity for each element
for i = 1:size(DT.ConnectivityList,1)
for j = 1:size(DT.ConnectivityList,2)
E_nodal(i,j) = E(DT.ConnectivityList(i,j)); %Assign E to each node within
each element
rho_nodal(i,j) = rho(DT.ConnectivityList(i,j));
end
E_elem(i) = mean(E_nodal(i,:)); %Find average E for each element
rho_elem(i) = mean(rho_nodal(i,:));
end
figure;
trimesh(DT.ConnectivityList,DT.Points(:,1),DT.Points(:,2),DT.Points(:,3),'E
dgeColor','k');
axis equal
title('Delaunay Triangulation of scaphod nodes')
%% Create material property sets
max_Modulus = max(E_elem);
min_Modulus = min(E_elem);

num_mat_bins = 20;

mat_bin_range =(max_Modulus-min_Modulus)/num_mat_bins;
for i = 1:length(E_elem)
elem_set_ID(i) = ceil((E_elem(i)-min_Modulus)/mat_bin_range);
end
Mat_dist = figure;
histogram(E_elem, num_mat_bins)
title('Distribution of element material properties')
figure;
histogram(elem_set_ID)
title('Distribution of element set ID')
xlabel('Material property (MPa)')
ylabel('Number of elements')
savefig([mat_file_path, '\', 'Mat_dist_smooth.fig'])
for i = 1:num_mat_bins
E_bin(i) = mean(E_elem(find(elem_set_ID == i)));
rho_bin(i) = mean(rho_elem(find(elem_set_ID == i)));
end

%%Find ligament nodal indexes
[NSET_nodes NSET_node_names] = ApplyBC_V2(mat_file_path,DT);

%%Convert Coords units from m to mm
Coords = Coords /1000;

%% Create .inp files v2

disp("Writing mesh")
file = fopen([mat_file_path, '\', 'MESH_AND_MAT_v5_smooth.inp'],'w');
model = mat_file_path(end-11:end-7);

fprintf(file, '*HEADING \r\nScaphoid %s\r\nUnits: Millimeters
(mm)\r\n',model);

for i = 1: num_mat_bins

fprintf(file, '**=====
=====\r\n');

```



```

fprintf(file, '**=====
=====\\r\\n');
    end

fclose(file);

%% Determine normal vectors for each ligament
NSET_Coords = cell(1,11);
for i = 1:11
    lig_nodes = Coords(NSET_nodes{1,i},:);
    if size(lig_nodes) > 2
        NSET_Coords{1,i} = fitNormal(lig_nodes);
    end
end

ligament_forces = [560 0 20 20 20 20 20 20 20 20 20];

NSET_COORDS_file = fopen([mat_file_path,
 '\\', 'NSET_NODAL_NORMAL_FORCES_v5_smooth.inp'], 'w');
fprintf(NSET_COORDS_file, '**BEGIN WRITING NODAL LIGAMENT FORCES \\r\\n');
for i = 1:11
    fprintf(NSET_COORDS_file, '*NSET,NSET=%s\\r\\n', NSET_node_names{1,i});
    fprintf(NSET_COORDS_file,
 '%d\\r\\n', ligament_forces(i) * NSET_Coords{1,i} / size(NSET_nodes{1,i}, 1));
    %%determines the nodal forces
    fprintf(NSET_COORDS_file, '**END WRITING NODE DATA\\r\\n');
end
fclose(NSET_COORDS_file);
% %%CHECK ELEMENT NUMBERING
%
scatter3(DT.Points(DT.ConnectivityList(1,:), 1), DT.Points(DT.ConnectivityList(1,:), 2), DT.Points(DT.ConnectivityList(1,:), 3))
%
text(DT.Points(DT.ConnectivityList(1,:), 1), DT.Points(DT.ConnectivityList(1,:), 2), DT.Points(DT.ConnectivityList(1,:), 3), {'1', '2', '3', '4'})

```

Appendix: Function to Map Ligaments to a Delaunay Triangle Mesh

```
%%scaphoid_DT -> delaunay triangle object containing both the node list and
%%connectivity list
function [NSET_nodes, NSET_node_names] = ApplyBC(file_path,scaphoid_DT)
TEMPLATE_SCAPHOID = 'F:\Master Thesis\Liem - Hons project\Right\MORPHED
STL\98048_sca_R_B_morphed_morphed.stl';
% SCAPHOID_FILE = 'F:\Master Thesis\Data from
Brown\14548\Models\sca_cropped.mat';
% load(SCAPHOID_FILE);

%Added with Rami on the 14th of July to get the mean shape of the SSM
SCAPHOID_NODES = load('F:\Master Thesis\Liem - Hons project\Right\MORPHED
STL\nodal_coords_pca_ready.mat');
v_all = SCAPHOID_NODES.V;
v_mean = mean(v_all);
v_mean_xyz = reshape(v_mean, [], 3);
v_mean_xyz_face = boundary(v_mean_xyz,0.99);

%Read template file
[f,v] = stlread_v2(TEMPLATE_SCAPHOID);

[v, f] = patchslim(v, f);

sourceV = v;
sourceF = f;

[registered3,sourceV,sourceF]=nonrigidICPv2(v_mean_xyz,sourceV,v_mean_xyz_f
ace,sourceF,6,1);

sourceV = sourceV - mean(sourceV); % shift centre to (0,0,0)

scaphoid_nodes = scaphoid_DT.Points;
scaphoid_connect = scaphoid_DT.ConnectivityList;

%% MORPHING TEMPLATE MESH TO INPUT STL

targetV = scaphoid_nodes;% input mesh
targetF = scaphoid_connect;
[targetV,IA,IC] = unique(targetV,'rows','legacy'); % delete any
redundant nodes
targetV = targetV - mean(targetV); % shift centre to (0,0,0)
targetF = boundary (targetV, 0.9);% redefine connectivity (elements)
surface_nodes = zeros(max(max(targetF)),3); %Create a matrix of zeros
for the number of nodes of the model
for i = targetF
    surface_nodes(i,:) = targetV(i,:); %Find the nodes on the surface
(these nodes are the nodes listed for surface triangulation)
end
surface_nodes = surface_nodes(any(surface_nodes,2),:); %Remove non zero
rows
surface_F = boundary(surface_nodes,0.9);
% STEP 1 - RIGID ICP

[targetV,sourceV,transform]=Preall(sourceV, targetV);
```

```

    [error,targetV,transform2] =
    rigidICP(sourceV,targetV,0,sourceF,targetF); % for aligning template with
    input mesh - rigidly

    [targetV,sourceV,transform]=Preall(sourceV, targetV);

    %targetV = (1/transform2.b) * targetV; %it appears that
    rigidICP_mesh_morph applies some scaling, so this is to reverse any scaling

%    model_range = range(targetV);
%    ssm_range = range(sourceV);
%
%    scaling_factor = model_range./ssm_range;
%
%    targetV = targetV./scaling_factor; %Rescaling scaphoid model to fit

% BOUNDARY CONDITION DEFINITIOSN
% DISTAL SCAPHOID CONTACT AREA
dscaphoid_centreIdx = knnsearch(sourceV,[12.25 -1.19 -0.8392]);
%Finding a node which is closest to the esimated centre
dscaphoid_centrePos = sourceV(dscaphoid_centreIdx,:); %Finding the node
closest to the estimated centre
dscaphoid = rangesearch(sourceV, dscaphoid_centrePos, 4.587); %Find
nodes within 69 square mm on statistical model

%RADIOSCAPHIOD CONTACT AREA
RS_centreIdx = knnsearch(sourceV,[-12.05 -0.8053 -0.8785]); %Finding a
node which is closest to the esimated centre
RS_centrePos = sourceV(RS_centreIdx,:); %Finding the node closest to
the estimated centre
RS = rangesearch(sourceV, RS_centrePos, 4.587); %Find nodes within 69
square mm on statistical model

%SCAPHIOCAPITATE LIGAMENT CONNECTION (ScC LIGAMENT)
ScC_centreIdx = knnsearch(sourceV,[4.924, -3.862, -3.609;3.716, -4.504,
-1.902;3.525, -5.013, 0.2449;3.365, -5.024, 1.481]); %Finding a node which
is closest to the esimated centre
ScC_centrePos = sourceV(ScC_centreIdx,:); %Finding the node closest to
the estimated centre
ScC = rangesearch(sourceV, ScC_centrePos, 1.8); %Find nodes within 59
square mm on statistical model (reduced radius to fit reference image)
ScC = [ScC{1,1} ScC{2,1} ScC{3,1} ScC{4,1}];
ScC = unique(ScC','rows','legacy');

%TRANSVERSE CARPAL LIGAMENT CONNECTION (TCL LIGAMENT)
TCL_centreIdx = knnsearch(sourceV,[6.132, 3.935, -4.553;7.373, 3.82, -
4.75;8.339, 3.842, -4.491]); %Finding a node which is closest to the
esimated centre
TCL_centrePos = sourceV(TCL_centreIdx,:); %Finding the nodes closest to
the estimated centre
TCL = rangesearch(sourceV, TCL_centrePos, 0.685); %Find nodes within
5.9 square mm on statistical model (some overlapping is added (1.5 times
the radius))
TCL = [TCL{1,1} TCL{2,1} TCL{3,1}];
TCL = unique(TCL','rows','legacy');

%RADIOSCAPHOLUNATE LIGAMENT CONNECTION (RSC LIGAMENT)

```

```

RSC_centreIdx = knnsearch(sourceV,[3.198, 4.128, -3.491;3.708, 4.958, -
3.71;4.097, 5.657, -3.796]); %Finding a node which is closest to the
esimated centre
RSC_centrePos = sourceV(RSC_centreIdx,:); %Finding the nodes closest to
the estimated centre
RSC = rangesearch(sourceV, RSC_centrePos, 0.685); %Find nodes within
5.9 square mm on statistical model (some overlapping is added (1.5 times
the radius))
RSC = [RSC{1,1} RSC{2,1} RSC{3,1}];
RSC = unique(RSC,'rows','legacy');

%VOLAR SCAPHOLUNATE INTEROSSEOUS LIGAMENT CONNECTION (VSL - vSLIO
LIGAMENT)
VSL_centreIdx = knnsearch(sourceV,[-8.347, -3.137, -4.922; -7.875, -
2.994, -4.969; -7.048, -2.818, -4.985]); %Finding a node which is closest
to the esimated centre
VSL_centrePos = sourceV(VSL_centreIdx,:); %Finding the nodes closest to
the estimated centre
VSL = rangesearch(sourceV, VSL_centrePos, 0.6); %Find nodes within 8.2
square mm on statistical model (some overlapping is added (1.5 times the
radius))
VSL = [VSL{1,1} VSL{2,1} VSL{3,1}];
VSL = unique(VSL,'rows','legacy');

%RADIO SCAPHOLUNATE LIGAMENT CONNECTION (RSL LIGAMENT)
RSL_centreIdx = knnsearch(sourceV,[-8.722, -1.94, -4.902]); %Finding a
node which is closest to the esimated centre
RSL_centrePos = sourceV(RSL_centreIdx,:); %Finding the node closest to
the estimated centre
RSL = rangesearch(sourceV, RSL_centrePos, 0.4); %Find nodes within 1.7
square mm on statistical model (reduced radius to fit reference image)
RSL = [RSL{1,1}];
RSL = unique(RSL,'rows','legacy');
%
% PROXIMAL SCAPHOLUNATE INTEROSSEOUS LIGAMENT CONNECTION (VSL - vSLIO
LIGAMENT) Considered insignificant - Greg -> membrane -> most likely
% will not have biomechanical effects
%
PSL_centreIdx = knnsearch(sourceV,[-10.87, -1.893, -3.489;-10.24, -
1.832, -3.959;-9.732, -1.551, -4.238;-9.144, -1.352, -4.53;-8.475, -1.178,
-4.764;-7.938, -0.8325, -4.826;-7.332, -0.7105, -4.777;-6.794, -0.6387, -
4.654]); %Finding a node which is closest to the esimated centre
%
PSL_centrePos = sourceV(PSL_centreIdx,:); %Finding the nodes closest
to the estimated centre
%
PSL = rangesearch(sourceV, PSL_centrePos, 0.485); %Find nodes within
21 square mm on statistical model (some overlapping is added (1.5 times the
radius))
%
PSL = [PSL{1,1} PSL{2,1} PSL{3,1} PSL{4,1} PSL{5,1} PSL{6,1} PSL{7,1}
PSL{8,1}];
%
PSL = unique(PSL,'rows','legacy');

%DORSAL SCAPHOLUNATE INTEROSSEOUS LIGAMENT CONNECTION (VSL - vSLIO
LIGAMENT)
DSL_centreIdx = knnsearch(sourceV,[-5.395, 7.751, 1.675; -6.049, 7.901,
1.391; -6.563, 8.04, 0.9814; -7.351, 7.897, 0.8122; -7.91, 7.798, 0.4]);
%Finding a node which is closest to the esimated centre
DSL_centrePos = sourceV(DSL_centreIdx,:); %Finding the nodes closest to
the estimated centre
DSL = rangesearch(sourceV, DSL_centrePos, 0.5); %Find nodes within 10.2
square mm on statistical model (some overlapping is added (1.5 times the
radius))
DSL = [DSL{1,1} DSL{2,1} DSL{3,1} DSL{4,1} DSL{5,1}];
DSL = unique(DSL,'rows','legacy');

```

```

%DORSAL INTERCARPAL LIGAMENT CONNECTION (RSL LIGAMENT)
DIC_centreIdx = knnsearch(sourceV, [-3.943, 4.364, 4.929; -2.984, 3.105,
5.678; -2.245, 2.386, 6.06; -1.42, 1.542, 6.414; -0.4322, 0.7376, 6.683]);
%Finding a node which is closest to the esimated centre
DIC_centrePos = sourceV(DIC_centreIdx,:); %Finding the node closest to
the estimated centre
DIC = rangesearch(sourceV, DIC_centrePos, 1.2); %Find nodes within 6.4
square mm on statistical model (reduced radius to fit reference image)
DIC = [DIC{1,1} DIC{2,1} DIC{3,1} DIC{4,1} DIC{5,1}];
DIC = unique(DIC, 'rows', 'legacy');

%SCAPHOTRAPEZIAL LIGAMENT (ScTm)
ScTm_centreIdx = knnsearch(sourceV, [9.924, -3.02, -4.381; 10.04, -3.88,
-3.895; 10.25, -4.471, -3.424; 9.968, -2.274, -4.669; 10.81 -6.023, -1.499;
10.78, -6.485, -0.1835; 11.18, -6.371, 1.023; 11.05, -6.058, 2.034]);
%Finding a node which is closest to the esimated centre
ScTm_centrePos = sourceV(ScTm_centreIdx,:); %Finding the nodes closest
to the estimated centre
ScTm = rangesearch(sourceV, ScTm_centrePos, 0.5);
ScTm = [ScTm{1,1} ScTm{2,1} ScTm{3,1} ScTm{4,1} ScTm{5,1} ScTm{6,1}
ScTm{7,1} ScTm{8,1}];
ScTm = unique(ScTm, 'rows', 'legacy');

%SCAPHOTRAPEZOIDAL LIGAMENT (ScTd)
ScTd_centreIdx = knnsearch(sourceV, [10.13, -0.578, -5.044; 9.874,
0.4472, -5.276; 9.533, 1.564, -5.441; 9.077, 2.518, -5.57]); %Finding a
node which is closest to the esimated centre
ScTd_centrePos = sourceV(ScTd_centreIdx,:); %Finding the nodes closest
to the estimated centre
ScTd = rangesearch(sourceV, ScTd_centrePos, 0.535); %Find nodes within
7.3 square mm on statistical model (some overlapping is added (1.5 times
the radius))
ScTd = [ScTd{1,1} ScTd{2,1} ScTd{3,1} ScTd{4,1}];
ScTd = unique(ScTd, 'rows', 'legacy');

%FLIP SSM MODEL ACROSS X AND Y AXIS
sourceV(:,1) = -sourceV(:,1);
sourceV(:,2) = -sourceV(:,2);
sourceV(:,3)=-sourceV(:,3);

% PLOT ALIGNED SCAPHOID MESH WITH TEMPLATE! USE FOR CHECKING ALIGNMENT
% Scaphoid_Morphing_Alignment = figure;
%
% subplot(1,3,1)
%
trisurf(surface_F,surface_nodes(:,1),surface_nodes(:,2),surface_nodes(:,3),
'facecolor','g','Edgecolor','none','FaceAlpha',0.5);
% hold on
%
trisurf(sourceF,sourceV(:,1),sourceV(:,2),sourceV(:,3),'facecolor',[0.1 0.2
0.8],'Edgecolor','none','FaceAlpha',0.5);
% light
% lighting phong;
% set(gca, 'visible', 'off')
% set(gcf, 'Color', [1 1 0.88])
% view(90,90)
% set(gca, 'DataAspectRatio', [1 1 1], 'PlotBoxAspectRatio', [1 1 1]);
%

```

```

% subplot(1,3,2)
%
trisurf(surface_F,surface_nodes(:,1),surface_nodes(:,2),surface_nodes(:,3),
'facecolor',[0.5 0.5 0.5],'Edgecolor','none','FaceAlpha',0.5);
% hold on
%
trisurf(sourceF,sourceV(:,1),sourceV(:,2),sourceV(:,3),'facecolor',[0.1 0.2
0.8],'Edgecolor','none','FaceAlpha',0.5);
% light
% lighting phong;
% set(gca, 'visible', 'off')
% set(gcf, 'Color', [1 1 0.88])
% view(0,0)
% set(gca, 'DataAspectRatio', [1 1 1], 'PlotBoxAspectRatio', [1 1 1]);
%
% subplot(1,3,3)
%
trisurf(surface_F,surface_nodes(:,1),surface_nodes(:,2),surface_nodes(:,3),
'facecolor',[0.5 0.5 0.5],'Edgecolor','none','FaceAlpha',0.5);
% hold on
%
trisurf(sourceF,sourceV(:,1),sourceV(:,2),sourceV(:,3),'facecolor',[0.1 0.2
0.8],'Edgecolor','none','FaceAlpha',0.5);
% light
% lighting phong;
% set(gca, 'visible', 'off')
% set(gcf, 'Color', [1 1 0.88])
% view(0,90)
% set(gca, 'DataAspectRatio', [1 1 1], 'PlotBoxAspectRatio', [1 1 1]);
%
% scrsz = [1,1,1920,1200];
%
% set(Scaphoid_Morphing_Alignment, 'Position', [1 1 scrsz(3) scrsz(4)])
% savefig([file_path, '\', 'Scaphoid_Morphing_Alignment.fig'])

% NON-RIGID ICP

[registered,surface_nodes,surface_F]=nonrigidICPv2(surface_nodes,sourceV,su
rface_F,sourceF,6,1); % for fitting (morphing) the template to the input
mesh = non-rigid, registered: mapped ligament nodes
%Plotting the ligaments onto the statistical model
statsitcal_mapping = figure;

trimesh(sourceF,sourceV(:,1),sourceV(:,2),sourceV(:,3),'EdgeColor','k','Fac
eColor',[0.6 0.6 0.6])
hold on
axis equal
scatter3(sourceV(RS{1,1},1),sourceV(RS{1,1},2),sourceV(RS{1,1},3),'b')

scatter3(sourceV(dscaphoid{1,1},1),sourceV(dscaphoid{1,1},2),sourceV(dscaph
oid{1,1},3),'r')
scatter3(sourceV(ScC,1),sourceV(ScC,2),sourceV(ScC,3),'y')
scatter3(sourceV(TCL,1),sourceV(TCL,2),sourceV(TCL,3),'r')
scatter3(sourceV(RSC,1),sourceV(RSC,2),sourceV(RSC,3),'m')
scatter3(sourceV(VSL,1),sourceV(VSL,2),sourceV(VSL,3),'c')
scatter3(sourceV(RSL,1),sourceV(RSL,2),sourceV(RSL,3),'r')
scatter3(sourceV(DSL,1),sourceV(DSL,2),sourceV(DSL,3),'c')
scatter3(sourceV(DIC,1),sourceV(DIC,2),sourceV(DIC,3),'m')
scatter3(sourceV(ScTm,1),sourceV(ScTm,2),sourceV(ScTm,3),'m')
scatter3(sourceV(ScTd,1),sourceV(ScTd,2),sourceV(ScTd,3),'m')

```

```

title('Mapping of ligaments on statistical model')
xlabel('Proximal to Distal');
ylabel('Volar to Dorsal');
zlabel('Radial to Ulnar');
hold off
savefig('SSM Ligament mapping')
%   %Plot mapped liagements and boundary conditions on model scaphoid
%   model_mapping = figure;
%
%
trimesh(surface_F,surface_nodes(:,1),surface_nodes(:,2),surface_nodes(:,3),
'FaceAlpha',1, 'EdgeColor', 'k')
%   hold on
%
%
scatter3(registered(RS{1,1},1),registered(RS{1,1},2),registered(RS{1,1},3),
'b') %Boundary condition of radioscaphoid joint - blue
%
scatter3(registered(dscaphoid{1,1},1),registered(dscaphoid{1,1},2),register
ed(dscaphoid{1,1},3),'r') %Area where force is applied - red
%
scatter3(registered(ScC{1,1},1),registered(ScC{1,1},2),registered(ScC{1,1},
3),'y')
%   scatter3(registered(TCL,1),registered(TCL,2),registered(TCL,3),'r')
%   scatter3(registered(RSC,1),registered(RSC,2),registered(RSC,3),'m')
%   scatter3(registered(VSL,1),registered(VSL,2),registered(VSL,3),'c')
%
scatter3(registered(RSL{1,1},1),registered(RSL{1,1},2),registered(RSL{1,1},
3),'r')
%   scatter3(registered(PSL,1),registered(PSL,2),registered(PSL,3),'r')
%   scatter3(registered(DSL,1),registered(DSL,2),registered(DSL,3),'c')
%
scatter3(registered(DICW,1),registered(DICW,2),registered(DICW,3),'m')
%
scatter3(registered(DICP,1),registered(DICP,2),registered(DICP,3),'m')
%
scatter3(registered(ScTm,1),registered(ScTm,2),registered(ScTm,3),'m')
%
scatter3(registered(ScTd,1),registered(ScTd,2),registered(ScTd,3),'m')
%   axis equal
%   hold off

%FIND SCAPHOID NODE INDEXES OF MAPPED LIGAMENTS
dscaphoid_scaphoidIdx =
knnsearch(surface_nodes,registered(dscaphoid{1,1},:));
dscaphoid_scaphoidIdx = unique(dscaphoid_scaphoidIdx, 'rows','legacy');

RSL_scaphoidIdx = knnsearch(surface_nodes,registered(RSL,:));
RSL_scaphoidIdx = unique(RSL_scaphoidIdx, 'rows','legacy');

RS_scaphoidIdx = knnsearch(surface_nodes,registered(RS{1,1},:));
RS_scaphoidIdx = unique(RS_scaphoidIdx, 'rows','legacy');

ScC_scaphoidIdx = knnsearch(surface_nodes,registered(ScC,:));
ScC_scaphoidIdx = unique(ScC_scaphoidIdx, 'rows','legacy');

TCL_scaphoidIdx = knnsearch(surface_nodes,registered(TCL,:));
TCL_scaphoidIdx = unique(TCL_scaphoidIdx, 'rows','legacy');

RSC_scaphoidIdx = knnsearch(surface_nodes,registered(RSC,:));
RSC_scaphoidIdx = unique(RSC_scaphoidIdx, 'rows','legacy');

```



```

VSL_scaphoidIdx = knnsearch(surface_nodes,registered(VSL,:));
VSL_scaphoidIdx = unique(VSL_scaphoidIdx, 'rows','legacy');

DSL_scaphoidIdx = knnsearch(surface_nodes,registered(DSL,:));
DSL_scaphoidIdx = unique(DSL_scaphoidIdx, 'rows','legacy');

DIC_scaphoidIdx = knnsearch(surface_nodes,registered(DIC,:));
DIC_scaphoidIdx = unique(DIC_scaphoidIdx, 'rows','legacy');

ScTd_scaphoidIdx = knnsearch(surface_nodes,registered(ScTd,:));
ScTd_scaphoidIdx = unique(ScTd_scaphoidIdx, 'rows','legacy');

ScTm_scaphoidIdx = knnsearch(surface_nodes,registered(ScTm,:));
ScTm_scaphoidIdx = unique(ScTm_scaphoidIdx, 'rows','legacy');

%CHECK SCAPHOID NODES VS MAPPED NODES
% figure;
%
trimesh(surface_F,surface_nodes(:,1),surface_nodes(:,2),surface_nodes(:,3),
'FaceAlpha',1, 'EdgeColor','k')
% hold on
% axis equal
%
scatter3(surface_nodes(RS_scaphoidIdx,1),surface_nodes(RS_scaphoidIdx,2),su
rface_nodes(RS_scaphoidIdx,3),'m')
%
scatter3(registered(RS{1,1},1),registered(RS{1,1},2),registered(RS{1,1},3),
'r')
%
%
scatter3(surface_nodes(ScC_scaphoidIdx,1),surface_nodes(ScC_scaphoidIdx,2),
surface_nodes(ScC_scaphoidIdx,3),'m')
%
scatter3(registered(ScC{1,1},1),registered(ScC{1,1},2),registered(ScC{1,1},
3),'r')
%
%
scatter3(surface_nodes(TCL_scaphoidIdx,1),surface_nodes(TCL_scaphoidIdx,2),
surface_nodes(TCL_scaphoidIdx,3),'m')
% scatter3(registered(TCL,1),registered(TCL,2),registered(TCL,3),'r')
%
%
scatter3(surface_nodes(RSC_scaphoidIdx,1),surface_nodes(RSC_scaphoidIdx,2),
surface_nodes(RSC_scaphoidIdx,3),'m')
% scatter3(registered(RSC,1),registered(RSC,2),registered(RSC,3),'r')
%
%
scatter3(surface_nodes(VSL_scaphoidIdx,1),surface_nodes(VSL_scaphoidIdx,2),
surface_nodes(VSL_scaphoidIdx,3),'m')
% scatter3(registered(VSL,1),registered(VSL,2),registered(VSL,3),'r')
%
%
scatter3(surface_nodes(PSL_scaphoidIdx,1),surface_nodes(PSL_scaphoidIdx,2),
surface_nodes(PSL_scaphoidIdx,3),'m')
% scatter3(registered(PSL,1),registered(PSL,2),registered(PSL,3),'r')
%
%
scatter3(surface_nodes(RSL_scaphoidIdx,1),surface_nodes(RSL_scaphoidIdx,2),
surface_nodes(RSL_scaphoidIdx,3),'m')

```

```

%
scatter3(registered(RSL{1,1},1),registered(RSL{1,1},2),registered(RSL{1,1},
3),'r')
%
%
scatter3(surface_nodes(DSL_scaphoidIdx,1),surface_nodes(DSL_scaphoidIdx,2),
surface_nodes(DSL_scaphoidIdx,3),'m')
%   scatter3(registered(DSL,1),registered(DSL,2),registered(DSL,3),'r')
%
%
scatter3(surface_nodes(DICP_scaphoidIdx,1),surface_nodes(DICP_scaphoidIdx,2
),surface_nodes(DICP_scaphoidIdx,3),'m')
%
scatter3(registered(DICP,1),registered(DICP,2),registered(DICP,3),'r')
%
%
scatter3(surface_nodes(DICW_scaphoidIdx,1),surface_nodes(DICW_scaphoidIdx,2
),surface_nodes(DICW_scaphoidIdx,3),'m')
%
scatter3(registered(DICW,1),registered(DICW,2),registered(DICW,3),'r')
%
%
scatter3(surface_nodes(ScTd_scaphoidIdx,1),surface_nodes(ScTd_scaphoidIdx,2
),surface_nodes(ScTd_scaphoidIdx,3),'m')
%
scatter3(registered(ScTd,1),registered(ScTd,2),registered(ScTd,3),'r')
%
%
scatter3(surface_nodes(ScTm_scaphoidIdx,1),surface_nodes(ScTm_scaphoidIdx,2
),surface_nodes(ScTm_scaphoidIdx,3),'m')
%
scatter3(registered(ScTm,1),registered(ScTm,2),registered(ScTm,3),'r')

%MAP NODES OF THE SURFACE ONLY SCAPHOID TO THE COMPLETE SCAPHOID MODE
[targetV,surface_nodes,transform]=Preall(surface_nodes,targetV);

[error,targetV,transform2] =
rigidICP(surface_nodes,targetV,0,surface_F,targetF); % for aligning
template with input mesh - rigidly
targetV = (1/transform2.b) * targetV; %it appears that
rigidICP_mesh_morph applies some scaling, so this is to reverse any scaling

rangeSSM = range(targetV);
rangeSSM_surface = range(surface_nodes);

surface_nodes(:,1) =
surface_nodes(:,1)*(rangeSSM(1,1)/rangeSSM_surface(1,1));
surface_nodes(:,2) =
surface_nodes(:,2)*(rangeSSM(1,2)/rangeSSM_surface(1,2));
surface_nodes(:,3) =
surface_nodes(:,3)*(rangeSSM(1,3)/rangeSSM_surface(1,3));
[targetV,surface_nodes,transform]=Preall(surface_nodes,targetV);

surface_nodes2 = zeros(max(max(targetF)),3); %Create a matrix of zeros
for the number of nodes of the model
for i = targetF
    surface_nodes2(i,:) = targetV(i,:); %Find the nodes on the surface
(these nodes are the nodes listed for surface triangulation)
end

```

```

    % knn_morph = knnsearch(surface_nodes2,surface_nodes); %Find nodes on
the scaphoid model which are closest to the surface_nodes.
%     figure;
%     trimesh(targetF,targetV(:,1),targetV(:,2),targetV(:,3),'FaceAlpha',0)
%     hold on
%
scatter3(targetV(knn_morph,1),targetV(knn_morph,2),targetV(knn_morph,3))
%     axis equal

    dscaphoid_scaphoidIdx =
knnsearch(surface_nodes2,surface_nodes(dscaphoid_scaphoidIdx,:));
    dscaphoid_scaphoidIdx = unique(dscaphoid_scaphoidIdx, 'rows','legacy');

    RSL_scaphoidIdx =
knnsearch(surface_nodes2,surface_nodes(RSL_scaphoidIdx,:));
    RSL_scaphoidIdx = unique(RSL_scaphoidIdx, 'rows','legacy');

    RS_scaphoidIdx =
knnsearch(surface_nodes2,surface_nodes(RS_scaphoidIdx,:));
    RS_scaphoidIdx = unique(RS_scaphoidIdx, 'rows','legacy');

    ScC_scaphoidIdx =
knnsearch(surface_nodes2,surface_nodes(ScC_scaphoidIdx,:));
    ScC_scaphoidIdx = unique(ScC_scaphoidIdx, 'rows','legacy');

    TCL_scaphoidIdx =
knnsearch(surface_nodes2,surface_nodes(TCL_scaphoidIdx,:));
    TCL_scaphoidIdx = unique(TCL_scaphoidIdx, 'rows','legacy');

    RSC_scaphoidIdx =
knnsearch(surface_nodes2,surface_nodes(RSC_scaphoidIdx,:));
    RSC_scaphoidIdx = unique(RSC_scaphoidIdx, 'rows','legacy');

    VSL_scaphoidIdx =
knnsearch(surface_nodes2,surface_nodes(VSL_scaphoidIdx,:));
    VSL_scaphoidIdx = unique(VSL_scaphoidIdx, 'rows','legacy');

    DSL_scaphoidIdx =
knnsearch(surface_nodes2,surface_nodes(DSL_scaphoidIdx,:));
    DSL_scaphoidIdx = unique(DSL_scaphoidIdx, 'rows','legacy');

    DIC_scaphoidIdx =
knnsearch(surface_nodes2,surface_nodes(DIC_scaphoidIdx,:));
    DIC_scaphoidIdx = unique(DIC_scaphoidIdx, 'rows','legacy');

    ScTd_scaphoidIdx =
knnsearch(surface_nodes2,surface_nodes(ScTd_scaphoidIdx,:));
    ScTd_scaphoidIdx = unique(ScTd_scaphoidIdx, 'rows','legacy');

    ScTm_scaphoidIdx =
knnsearch(surface_nodes2,surface_nodes(ScTm_scaphoidIdx,:));
    ScTm_scaphoidIdx = unique(ScTm_scaphoidIdx, 'rows','legacy');

    Scaphoid_ligament_mapping = figure;

trimesh(targetF,targetV(:,1),targetV(:,2),targetV(:,3),'EdgeColor','k','FaceColor',[0.6 0.6 0.6])
    hold on
    axis equal

```

```

scatter3(targetV(dscaphoid_scaphoidIdx,1),targetV(dscaphoid_scaphoidIdx,2),
targetV(dscaphoid_scaphoidIdx,3),'r')

scatter3(targetV(RS_scaphoidIdx,1),targetV(RS_scaphoidIdx,2),targetV(RS_sca
phoidIdx,3),'b')

scatter3(targetV(ScC_scaphoidIdx,1),targetV(ScC_scaphoidIdx,2),targetV(ScC_
scaphoidIdx,3),'y')

scatter3(targetV(TCL_scaphoidIdx,1),targetV(TCL_scaphoidIdx,2),targetV(TCL_
scaphoidIdx,3),'r')

scatter3(targetV(RSC_scaphoidIdx,1),targetV(RSC_scaphoidIdx,2),targetV(RSC_
scaphoidIdx,3),'m')

scatter3(targetV(VSL_scaphoidIdx,1),targetV(VSL_scaphoidIdx,2),targetV(VSL_
scaphoidIdx,3),'c')

scatter3(targetV(RSL_scaphoidIdx,1),targetV(RSL_scaphoidIdx,2),targetV(RSL_
scaphoidIdx,3),'r')

scatter3(targetV(DSL_scaphoidIdx,1),targetV(DSL_scaphoidIdx,2),targetV(DSL_
scaphoidIdx,3),'c')

scatter3(targetV(DIC_scaphoidIdx,1),targetV(DIC_scaphoidIdx,2),targetV(DIC_
scaphoidIdx,3),'m')

scatter3(targetV(ScTd_scaphoidIdx,1),targetV(ScTd_scaphoidIdx,2),targetV(Sc
Td_scaphoidIdx,3),'m')

scatter3(targetV(ScTm_scaphoidIdx,1),targetV(ScTm_scaphoidIdx,2),targetV(Sc
Tm_scaphoidIdx,3),'m')
    title('Mapping of ligaments onto scaphoid model')
    xlabel('Proximal to Distal');
    ylabel('Volar to Dorsal');
    zlabel('Radial to Ulnar');
    hold off
    %savefig([file_path,'\','Scaphoid_ligament_mapping_smooth.fig'])
    %PRINT NODE SETS
    NSET = cell(1,11);
    NSET{1,1} = dscaphoid_scaphoidIdx;
    NSET{1,2} = RS_scaphoidIdx;
    NSET{1,3} = ScC_scaphoidIdx;
    NSET{1,4} = TCL_scaphoidIdx;
    NSET{1,5} = RSC_scaphoidIdx;
    NSET{1,6} = VSL_scaphoidIdx;
    NSET{1,7} = RSL_scaphoidIdx;
    NSET{1,8} = DSL_scaphoidIdx;
    NSET{1,9} = DIC_scaphoidIdx;
    NSET{1,10} = ScTd_scaphoidIdx;
    NSET{1,11} = ScTm_scaphoidIdx;

    NSET_names = cell(1,11);
    NSET_names{1,1} = 'dscaphoid';
    NSET_names{1,2} = 'RS';
    NSET_names{1,3} = 'ScC';
    NSET_names{1,4} = 'TCL';
    NSET_names{1,5} = 'RSC';
    NSET_names{1,6} = 'VSL';

```

```
NSET_names{1,7} = 'RSL';  
NSET_names{1,8} = 'DSL';  
NSET_names{1,9} = 'DICW';  
NSET_names{1,10} = 'ScTd';  
NSET_names{1,11} = 'ScTm';  
  
NSET_nodes = NSET;  
NSET_node_names = NSET_names;
```

end